

FINAL  
CONTRACT REPORT  
VTRC 09-CR13

**FIELD TESTING OF THE WOLF CREEK  
CURVED GIRDER BRIDGE:  
PART I:  
VIBRATION TESTS**

ROBERT S. TURNAGE  
Graduate Research Assistant

THOMAS T. BABER  
Associate Professor

Department of Civil and Environmental Engineering  
University of Virginia



**Standard Title Page - Report on Federally Funded Project**

1. Report No.: FHWA/VTRC 09-CR13		2. Government Accession No.:		3. Recipient's Catalog No.:	
4. Title and Subtitle: Field Testing of the Wolf Creek Curved Girder Bridge: Part I: Vibration Tests				5. Report Date: June 2009	
				6. Performing Organization Code:	
7. Author(s): Robert S. Turnage and Thomas T. Baber				8. Performing Organization Report No.: VTRC 09-CR13	
9. Performing Organization and Address: Virginia Transportation Research Council 530 Edgemont Road Charlottesville, VA 22903				10. Work Unit No. (TRAIS):	
				11. Contract or Grant No.: 83146	
12. Sponsoring Agencies' Name and Address: Virginia Department of Transportation      Federal Highway Administration 1401 E. Broad Street                              400 North 8th Street, Room 750 Richmond, VA 23219                                Richmond, VA 23219-4825				13. Type of Report and Period Covered: Final Contract	
				14. Sponsoring Agency Code:	
15. Supplementary Notes: This project (including both the Part I and Part II studies) was financed with federal Part II State Planning and Research (SPR) funds at an estimated cost of \$155,147					
16. Abstract:  <p>The Wolf Creek Bridge is a curved, multi-girder three span steel composite bridge located south of Narrows, Virginia, that was completed in 2006. A finite element model of the bridge revealed that pier flexibility may be important in modeling the bridge. In addition, questions have been raised as to the effectiveness of the C15x33 diaphragms in providing lateral transfer of loads between members.</p> <p>This study was conducted as Phase I of a project for which the overall goal was to use field testing to obtain a better understanding of the behavior of multi-span curved girder bridges. An array of vertically oriented accelerometers was located along the inner and outer edges of the bridge, along with radially oriented accelerometers along the outer edge, a tangentially oriented accelerometer on the outer edge, and an additional vertical accelerometer placed in the middle of the center span. Dynamic response data were collected under a variety of excitations, including sinusoidal forcing induced by an electro-dynamic shaker, impulse loadings at various locations, and several different vehicular loads.</p> <p>The dynamic data were transformed into the frequency domain and analyzed using a simple frequency domain algorithm to extract vibration frequencies and mode shapes. The resulting frequencies and mode shapes were compared with the existing finite element model. The findings indicated that not only is pier flexibility important, as had been hypothesized, but also that end constraints imposed by highway guardrails change both the natural frequencies and the mode shapes in ways that had not been anticipated. Frequencies of modes with strong pier participation and modes with strong transverse (hogging) components were lower than predicted by the computer model, suggesting that pier stiffness may be less than the model predicted and that transverse stiffness, to which the diaphragms contribute, may also be estimated.</p> <p>Implications of this study could have a significant effect on future health monitoring applications as they pertain to both curved girder bridges correctly. Thus, it will be important to perform subsequent numerical research studies to develop models that will result in more precise predictions and to use these and other methods being developed in any health monitoring applications.</p>					
17 Key Words: Curved steel girder bridges, field testing, finite element modeling, strain measurements			18. Distribution Statement: No restrictions. This document is available to the public through NTIS, Springfield, VA 22161.		
19. Security Classif. (of this report): Unclassified		20. Security Classif. (of this page): Unclassified		21. No. of Pages: 67	22. Price:

**FINAL CONTRACT REPORT**

**FIELD TESTING OF THE WOLF CREEK CURVED GIRDER BRIDGE:  
PART I: VIBRATION TESTS**

**Robert S. Turnage**  
**Graduate Research Assistant**

**Thomas T. Baber**  
**Associate Professor**

**Department of Civil and Environmental Engineering**  
**University of Virginia**

*Project Manager*

Jose P. Gomez, Ph.D., P.E., Virginia Transportation Research Council

Contract Research Sponsored by  
the Virginia Transportation Research Council  
(A partnership of the Virginia Department of Transportation  
and the University of Virginia since 1948)

In Cooperation with the U.S. Department of Transportation  
Federal Highway Administration

Charlottesville, Virginia

June 2009  
VTRC 09-CR13

## **DISCLAIMER**

The project that is the subject of this report was done under contract for the Virginia Department of Transportation, Virginia Transportation Research Council. The contents of this report reflect the views of the authors, who are responsible for the facts and the accuracy of the data presented herein. The contents do not necessarily reflect the official views or policies of the Virginia Department of Transportation, the Commonwealth Transportation Board, or the Federal Highway Administration. This report does not constitute a standard, specification, or regulation. Any inclusion of manufacturer names, trade names, or trademarks is for identification purposes only and is not to be considered an endorsement.

Each contract report is peer reviewed and accepted for publication by Research Council staff with expertise in related technical areas. Final editing and proofreading of the report are performed by the contractor.

Copyright 2009 by the Commonwealth of Virginia.  
All rights reserved.

## ABSTRACT

The Wolf Creek Bridge is a curved, multi-girder three span steel composite bridge located south of Narrows, Virginia, that was completed in 2006. A finite element model of the bridge revealed that pier flexibility may be important in modeling the bridge. In addition, questions have been raised as to the effectiveness of the C15x33 diaphragms in providing lateral transfer of loads between members.

This study was conducted as Phase I of a project for which the overall goal was to use field testing to obtain a better understanding of the behavior of multi-span curved girder bridges. An array of vertically oriented accelerometers was located along the inner and outer edges of the bridge, along with radially oriented accelerometers along the outer edge, a tangentially oriented accelerometer on the outer edge, and an additional vertical accelerometer placed in the middle of the center span. Dynamic response data were collected under a variety of excitations, including sinusoidal forcing induced by an electro-dynamic shaker, impulse loadings at various locations, and several different vehicular loads.

The dynamic data were transformed into the frequency domain and analyzed using a simple frequency domain algorithm to extract vibration frequencies and mode shapes. The resulting frequencies and mode shapes were compared with the existing finite element model. The findings indicated that not only is pier flexibility important, as had been hypothesized, but also that end constraints imposed by highway guardrails change both the natural frequencies and the mode shapes in ways that had not been anticipated. Frequencies of modes with strong pier participation and modes with strong transverse (hogging) components were lower than predicted by the computer model, suggesting that pier stiffness may be less than the model predicted and that transverse stiffness, to which the diaphragms contribute, may also be estimated.

Implications of this study could have a significant effect on future health monitoring applications as they pertain to both curved and straight girder bridges. It is essential that finite element models in such long-term applications be able to reproduce the “as-built” response characteristics of a bridge. The current study raised significant issues about the ability to model the behavior of curved girder bridges correctly. Thus, it will be important to perform subsequent numerical research studies to develop models that will result in more precise predictions and to use these and other methods being developed in any health monitoring applications.

# FINAL CONTRACT REPORT

## FIELD TESTING OF THE WOLF CREEK CURVED GIRDER BRIDGE: PART I: VIBRATION TESTS

**Robert S. Turnage**  
**Graduate Research Assistant**

**Thomas T. Baber**  
**Associate Professor**

**Department of Civil and Environmental Engineering**  
**University of Virginia**

### INTRODUCTION

Since the early 1990s, horizontally curved girder bridges have represented more than one fourth of the bridges constructed in the United States (Linzell, 2004). The widespread use of such bridges stems primarily from the need to fit large, complex, highway interchanges into densely populated areas throughout the country, a need that is most efficiently met by using curved superstructure alignments. Because of their curved alignments, torsion and vertical bending do not decouple in curved girder bridges, but occur simultaneously under loading. Curved webs behave like shells instead of plates under load, and tend to bend out of plane. Steel I-girders are commonly used in curved bridges due to their constructability, but they have relatively low torsional stiffness due to their open web sections, and the thin plates used in their construction. Therefore cross frames or diaphragms are used to provide lateral support for the girders. The cross-frames or diaphragm members transfer load from inner girders to outer girders, and hence act as primary structural members.

The earliest studies on curved girder bridges in the United States were conducted beginning in the late 1960s by the Pennsylvania Department of Transportation (PDOT) financed by the Federal Highway Administration (FHWA) through the Consortium University Research Team (CURT) Project. The project's findings were incorporated into the American Association of State Highway and Transportation Officials (AASHTO) first *Guide Specifications for Horizontally Curved Highway Bridges* in 1976 (Hall, 1996). After eight revisions over the next two decades, the second edition of the guide specifications was published in 1993, but it was criticized for not addressing many important issues that had plagued the first edition, including a clarification of the preliminary analysis methods and erection procedures. The only other set of guidelines dealing with this curved girder bridge design is the *Guidelines for the Design of Horizontal Curved Girder Bridges*, also known as the *Hanshin Guidelines*, which was developed contemporarily to the AASHTO specifications as an addition to the Japanese Road Association Specifications for Highway Bridges.

Unfortunately, practicing engineers have generally perceived the guide specifications as being overly difficult to interpret, noting that the commentary lacked detail, that the supporting materials were hard to obtain, and that no examples were included until recently. Although no failures or performance problems have been directly associated with the guide specifications, efforts to improve them were initiated with the Curved Steel Bridge Research Project (CSBRP) in 1992 due to the issues with interpreting the guidelines, and their perceived overly conservative nature. The CSBRP project was undertaken following a report by Task Group 14 of the Structural Stability Research Council on Horizontally Curved Girders that enumerated the extensive problems with the current specifications and proposed research to rectify them. Specifically this project set out to compare finite element models to laboratory testing done on full scale Curved I Girders. The following year, the National Cooperative Highway Research Program (NCHRP) initiated project NCHRP 12-38 to improve specifications for Load Factor Design (LFD) and construction principles. The design recommendations from that project were adopted as part of the 2003 AASHTO guide specifications, which extended design equations to include combined vertical bending, lateral bending, torsion and shear stresses, and recommended further research into horizontally curved girder bridges.

The guidelines have met with general approval, however there has been some commentary about the NCHRP Project 12-38 not including the execution of any new research to improve any of the specifications, and particularly that the provisions are “likely extremely conservative . . . due to a lack of complete knowledge of the implications on curved bridge performance” (Linzell, 2004), and one research project found that all bridges that were tested were conservative by 70-82% for single trucks (McElwain, 2000).

### **Previous Studies**

Since the inception of the CURT project in the 1960s, a major focus has been placed on the dynamic analyses of curved girder bridges. Although much of the research has been primarily analytical, several projects have been undertaken to conduct vibration tests on different types of bridges. According to Christiano and Culver (1969), the first three such projects were reported in the mid-1960s. Soto (1966) performed full-scale dynamic tests on a curved girder suspended bridge in Washington D.C, comparing the measured response to the analytical methods available at that time. Clark (1966) produced a scale model of a two-span curved girder bridge with rolled I-beams and a continuous concrete deck for dynamic testing, while Roll and Aneja (1966) performed tests on a plastic model of a box beam.

Culver and Christiano (1969) conducted two concurrent projects that performed static and dynamic analyses of a curved girder bridge. They created a small scale model of an existing curved girder highway interchange consisting of two spans with a pair of curved plexiglass plate girders connected by sixteen evenly spaced diaphragms. The deck was also modeled with a sheet of plexiglass. In the first project, they recorded the stresses and deflections under static loading. Christiano and Culver (1969) adapted the static analysis of Dabrowski (1968) to include dynamic loading under moving sprung and un-sprung masses. The masses and speeds of the four-wheeled carriage were varied to examine the dynamic effects. In particular, they analyzed and discussed the “triple coupling phenomenon” of bending and twisting modes that curved

girder bridges experience and considered specific parameters that appear in the coupling. They also noted that the warping moments showed a larger dynamic amplification than the bending moments.

Armstrong (1972) conducted dynamic tests on two curved girder bridges on the Huyck Stream in Rensselaer, New York. The first bridge was a two-span continuous bridge while the second was a single span, and both were considered to be prototype structures enabling their comparison to simplified design techniques. For the tests, the project utilized a three-axle tractor and semi-trailer configuration that featured axle loadings of 10.0, 34.4, and 32.9-kips to create the desired deflections and vibrations for recording. It was concluded that the bottom of the cross-braced cross frames play a significant role in forcing the girders to act as a single system, and that the outer girder had a significantly greater dynamic response than the inner girders.

Shear connectors were examined by Colville (1973) who loaded four curved composite beams of varying girder size and radius of curvature to failure. Deflections, strains, rotations, and the slip between the two materials were measured on the simple span beams. Two of the beams failed in torsion at the supports and the other two beams failed in a combination of torsion and bending stress at mid-span. The report concluded that the design method that had been utilized was unable to accurately predict the deflections of the beams and demonstrated the influence of the radius of curvature on the eccentricity of the longitudinal force caused by a normal bending stress and the vertical force in the shear connectors due to the developed torsion.

Following the creation of the CSBRP in 1992, experimentation on curved girder bridges resumed in earnest. Shanmugam et al. (1995) conducted tests on a series of models of both rolled and built-up I-beams with varying radii of curvature. Setting out to test for ultimate strength and deflections and compare them to a finite element analysis, they considered the effects of residual stresses and showed that the load-carrying capacity of the bridge was proportional to the ratio of radius of curvature to span length, as earlier studies had assumed.

Littler (1995) assessed different methods for estimating damping from full-scale tests. His article primarily dealt with tall buildings, and never considered curved girders, but it does touch on some difficulties encountered with trying to extract damping estimates that can be applied to both curved girder bridges and straight girder bridges. The most relevant point he makes is that ensemble averaging of ambient data only works in theory due to the large amount of data required, and steady-state forced vibration procedures are only accurate if extensive knowledge of the wind speed and direction on site is available as well as the forced vibration input.

While the early studies tended to feature experiments with fixed supports that only loaded the girders within their elastic range, Zureick et al. (2000) designed a full-scale three girder, simple span bridge for laboratory testing and loaded the outermost girder through the full inelastic range. The project primarily focused on determining the resulting stresses in the built-up cross frames between the girders.

A change in direction of curved girder bridge research began around 2000 when additional projects were developed to perform tests on in-service bridges. McElwain and Laman

(2000) conducted field studies on in-service, curved, steel, I-girder bridges of one, two and three spans. They recorded data under a heavy test truck as well as the bridges' normal traffic loading. They then calculated the allowable dynamic load and transverse bending distribution factors and compared them to results obtained from numerical grillage models. The transverse bending moment distribution factors were regarded as especially important to the study because of the need for the curved girders to resist torsional moment. They found that the AASHTO specifications were conservative, especially under a single truck loading, while the numerical models were reasonably accurate compared to the bridge data.

Womack et al. (2001) carried out static and dynamic tests on a three-span curved, steel girder bridge scheduled for demolition. The bridge was tested with three different boundary conditions to analyze the effect of boundary conditions on the modal analysis as well as to verify the accuracy of a finite element model. Influence diagrams were constructed from the tests and compared favorably to the models. The different boundary conditions were shown to have a decided effect on the natural frequencies and mode shapes of the structure.

Linzell (2004) performed nine studies on six different laboratory scale framing plans to assess the capability of analysis tools to predict bridge response during erection. The different studies were not meant to represent the typical field assembly process, but rather to see if the order of the assembly affected the response and stresses of the girders. While comparisons to the finite element models were reported to be favorable, it is noteworthy that the models occasionally under-predicted the stresses in the interior girders.

Zivanovic (2005) performed dynamic tests on a full-scale, box-girder foot bridge and compared it to a finite element model. He observed that the primary influence on the vertical and horizontal bending modes are, respectively, the boundary conditions representing the end supports, specifically in the longitudinal direction, and the bending stiffness of the support columns.

## **The Wolf Creek Bridge**

### **Bridge Location and Specifications**

The Wolf Creek Bridge is a two-lane, three-span, curved girder bridge measuring 190 ft 2 in, including the abutments, with a radius of curvature of 260.0-feet at the centerline. It is located on Route 644, just off Virginia State Road 61, in Bland County, Virginia. The bridge was designed using the 1996 American Association of State Highway Transportation Officials (AASHTO) Standard Specifications for Highway Bridges with 1997 and 1998 Interim Specifications and VDOT Modifications and built using the 2002 VDOT *Road and Bridge Specifications* and the 2001 VDOT *Road and Bridge Standards*. Detailed design calculations on the Wolf Creek Bridge were carried out using the design optimization software MDX. The bridge was completed in 2006. This bridge is an ideal subject for field study due to its isolated location and limited traffic volume as well as its symmetric, multi-span geometry.

## Substructure

The Wolf Creek Bridge has two symmetrically placed hammerhead piers, creating two end spans of 56 ft and a center span of 76 ft. The piers were constructed using class A3, 3000-psi concrete and feature a 26 ft-0 in wingspan aligned along the radius of the curved bridge, resting upon a single 5 ft-0 in diameter column that rises 15 ft- ½ in above a 3 ft thick, 10 ft square foundation. Altogether, the piers have a total height of 24 ft-8 ½ in at their outer edge and 24 ft-3 ½ in on their inner edge.

The pier caps are 30 in thick and are effectively tilted a total of five inches towards the inside curve of the bridge, as shown in Figure 1, creating the required super-elevation for the curved deck above. In order to achieve the necessary slope from the northern bank to the southern bank, hereafter referenced as the left and right ends of the bridge, when viewed from the center of curvature, the left pier footing is located ¾ in higher than the right pier footing.

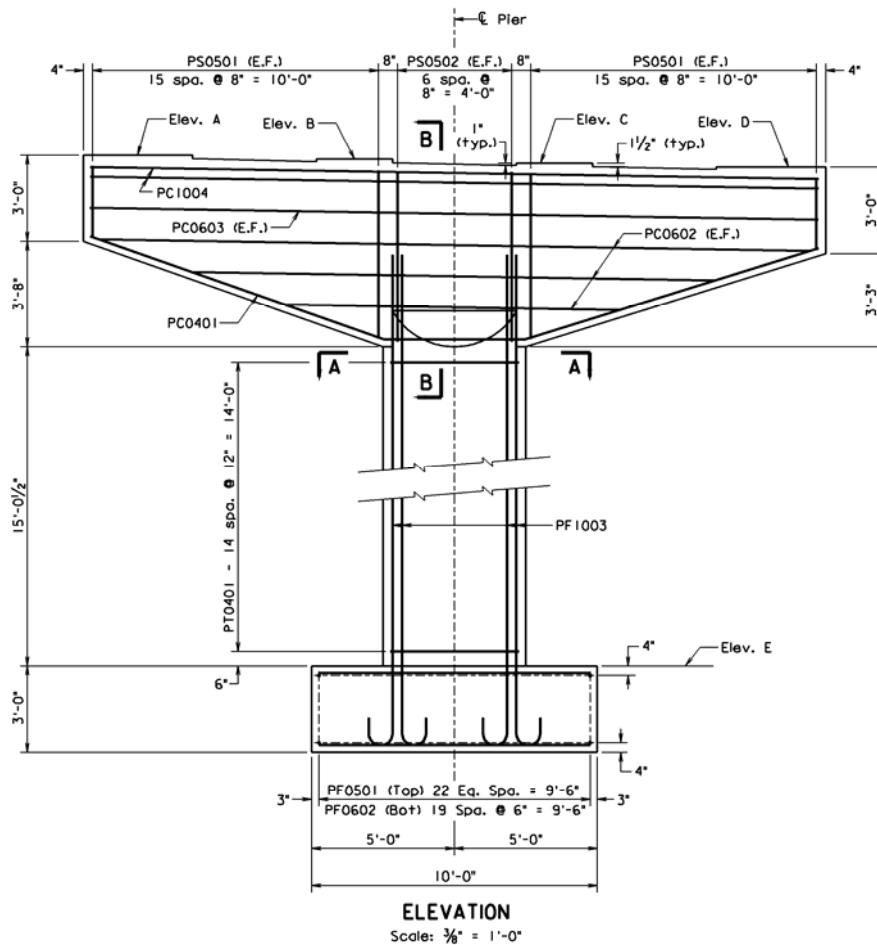


Figure 1. Pier Elevation Detail

## Superstructure

The framing plan for the Wolf creek bridge superstructure is shown in Figure 2. Details of the superstructure are discussed below.







**Figure 4. Guardrail Attachment**

In order to allow for thermal expansion, a preformed, elastomeric sealer is attached between the deck and the abutments on both sides of the bridge. In its uncompressed state, it is 3-inches wide, 3-inches tall, and extends the full width of the bridge in one piece, but when installed it is compressed into a 1-7/8-inch wide gap at the end of the bridge.

## **Finite Element Modeling**

### *Synopsis and Limitations of Superstructure Model*

Lydzinski (2006) developed a detailed finite element model of the Wolf Creek Bridge using the commercial software ANSYS. He studied the effects of altering the boundary conditions of the model upon the dynamic characteristics of the bridge, including determining the natural frequencies and mode shapes. His thesis was intended to provide an a priori model for the current project, one of the objectives of which is to establish a validated computational test bed for subsequent numerical studies. Since a major objective of the current study is to use the results of field dynamic testing to assess the accuracy of the model's assumptions and ability to model the dynamics of this bridge, Lydzinski's model will be discussed in some detail.

Lydzinski began by conducting convergence studies for the girders, the diaphragms, the varying girder cross sections, and the concrete deck. (Lydzinski, 2006). The superstructure model was created entirely using SHELL63 elements. The licensed version of the program only permitted about thirty thousand degrees of freedom, which limited the ability to model the bridge's piers fully. Other approximations that Lydzinski noted were the modeling of the bearing components between the girders and piers as well as the connections between the girder and diaphragm members. The girders were directly connected to the piers through a contact node, and Lydzinski hypothesized that it was probable that the bearings may have a significant effect on the dynamic characteristics of the bridge. Similarly, even though there are connection plates welded to the girders and then bolted to the diaphragms, the model represents the connection plates and diaphragms as a single entity, effectively ignoring any potential slip of the bolted connections. While nothing was done directly in the current tests to determine the validity of this approximation, certain differences between the field data and the computer predictions suggest a lack of complete rigidity, which will be further discussed subsequently.

## *Pier Models*

The main focus of Lydzinski's research that is relevant to this paper was the creation of two models of the bridge in order to examine the effect of modeling the central piers as rigid supports. Many current computer design programs for horizontally curved bridges assume that the interior supports of the bridge are equivalent to ideal pinned connections. Although several design programs do permit flexible support conditions as a design option, no systematic means are typically provided for explicitly including the substructure as part of the design model.

Lydzinski's first finite element model ignored pier flexibility, simply providing pinned and roller supports under the appropriate support points on the superstructure. This model will be referred to as the *rigid pier model*. This modeling approach is fairly common practice in bridge design but, according to Lydzinski's research, may have "created significant inaccuracies" and was intended as a baseline model for comparison with more complete analyses (Lydzinski, 2006).

In order to reduce the size of the final model, the piers were first modeled separately using tetrahedral elements in order to provide a basis for constructing a simplified pier model. The large pier model used 21,941 nodes and 14,361 individual SOLID95 elements (Lydzinski, 2006). Lydzinski's pier model did not include pier cracking, nor did it attempt to explicitly include reinforcement, but assumed that the pier behaved effectively as if it were un-cracked.

Since modeling the two piers alone would have exceeded the allowed number of degrees of freedom, a beam-element model was then created using the same concrete properties, but only having 32 ANSYS BEAM4 elements. In Lydzinski's final model, the pier stiffness was more closely modeled than pier mass. This was considered acceptable, since the overall mass of the structure is dominated by the superstructure mass. The influence of overall pier flexibility upon the bridge dynamic characteristics was investigated using the beam model only.

## *Generated Natural Frequencies and Mode Shapes*

Lydzinski (2006) used his models to predict the first twenty natural frequencies and mode shapes of the bridge and compare their differences as a means of examining the accuracy of modeling the central piers as rigid supports. This includes all modes generated up to about 20 Hz, the range where it was felt that the field data were the most likely to produce identifiable mode shapes. Comparison of Lydzinski's predicted frequencies and mode shapes with measured frequencies and mode shapes is an important part of the current project, so his frequencies are tabulated subsequently as part of the discussion. The frequencies predicted by the two models showed striking differences. Lydzinski pointed out that the model with piers introduces additional mode shapes that the simply supported model does not allow, including the mode shapes corresponding to the first two natural frequencies.

Lydzinski subsequently compared the mode shapes that could be identified as having similar shapes between the two models. Typically, wherever the mode shape could allow pier participation, the flexible pier model produced natural frequencies at least 1 Hz lower, and pier displacement was evident in many of the modes. This was particularly true of the modes that

may be described as combined vertical bending– torsion modes, an important observation since these modes are often among the dominant response modes under vehicular loadings. In the presence of the flexible piers, these modes introduced both twisting and lateral displacement of the pier caps, suggesting that a non-negligible change in the distribution of positive and negative bending moments may occur.

## **PURPOSE AND SCOPE**

The overall objective of the current study was to critically evaluate and update the FE models of the Wolf Creek bridge using measured field vibration data, in order to improve our understanding of the behavior and modeling of such bridges. The objective was achieved by carrying out several tasks.

The first task was to perform vibration tests on the Wolf Creek Bridge and to use the analyzed data to construct natural frequency and mode shape information. The strategy used for this task was to deploy an array of accelerometers on the bridge, and subject the bridge to a variety of dynamic loadings. The collected vibration data were transformed into the frequency domain using the Fast Fourier Transform (FFT) to determine as many natural frequencies and respective mode shapes as possible.

The second task was to compare the measured frequencies and mode shapes with the corresponding values predicted by the FE models to form the basis for constructing an improved computational test bed model for the bridge. The objectives of the comparison were to critically evaluate the accuracy of the FE analysis of the bridge, to provide some insight as to the reasons for any observed inaccuracies, and when specific sources of discrepancies could be identified to modify the FE model in order to improve its performance.

## **METHODS**

### **Testing Equipment and Procedure**

#### **Accelerometers**

To measure the dynamic response of the Wolf Creek Bridge, two types of accelerometers were used. PCB 393C seismic accelerometers were used to measure the vertical motion of the bridge. The accelerometers weigh 31.2-ounces each, which is negligible relative to the bridge weight. They have a sensitivity of 1 Volts per g – plus or minus 15% – and a broadband resolution of 0.001g rms, with g being the acceleration due to gravity. The primary frequency range is 0.025-Hz to 800-Hz, with an accuracy of plus or minus 5% within that range. Since the lowest frequency of interest is thought to be above 2 Hz, based upon Lydzinski's flexible pier model, the frequencies of interest are within the primary range.

The second type of accelerometer used in the project is a PCB 302B03 Quartz Compression, Inverted Accelerometer. The 302B03 accelerometer weighs about 1.4 ounces.

The center portion of the 302B03 housing is a hexagon shape, allowing it to be laid on its side. With only a 300-milivolt per g sensitivity – plus or minus 2% – and resolution of 0.0025 g it is not as well suited for this study as the 393C, but its shape has one major advantage – laying it on its side allows lateral motion to be recorded while the 393C can only record vertical vibrations unless special mounting fixtures are used.

Also of concern is that the primary frequency range of the 302B03 accelerometers is from 2.5-Hz to 500-Hz, and secondary frequency range from 1.5-Hz to 7000-Hz. Since at least one of Lydzinski’s predicted frequencies lies outside the primary frequency range of the 302B03 accelerometers, tests were conducted to compare the performance of this accelerometer to the 393C. These tests consisted of attaching the accelerometers to the top of an electrodynamic shaker and recording data at driven frequencies ranging from 0.5-Hz to 15-Hz and noting their amplitudes and phase angles. In these tests, while the measured amplitudes showed no significant difference after correcting for sensitivity differences, the phase angle change between the two types of accelerometers was pronounced at the lower frequencies as is shown in Figure 5. Since the finite element model predicts that this project may find frequencies as low as 2.3-Hz, the phase angle shift must be taken into consideration in determining the correct phase angles of the mode shapes.

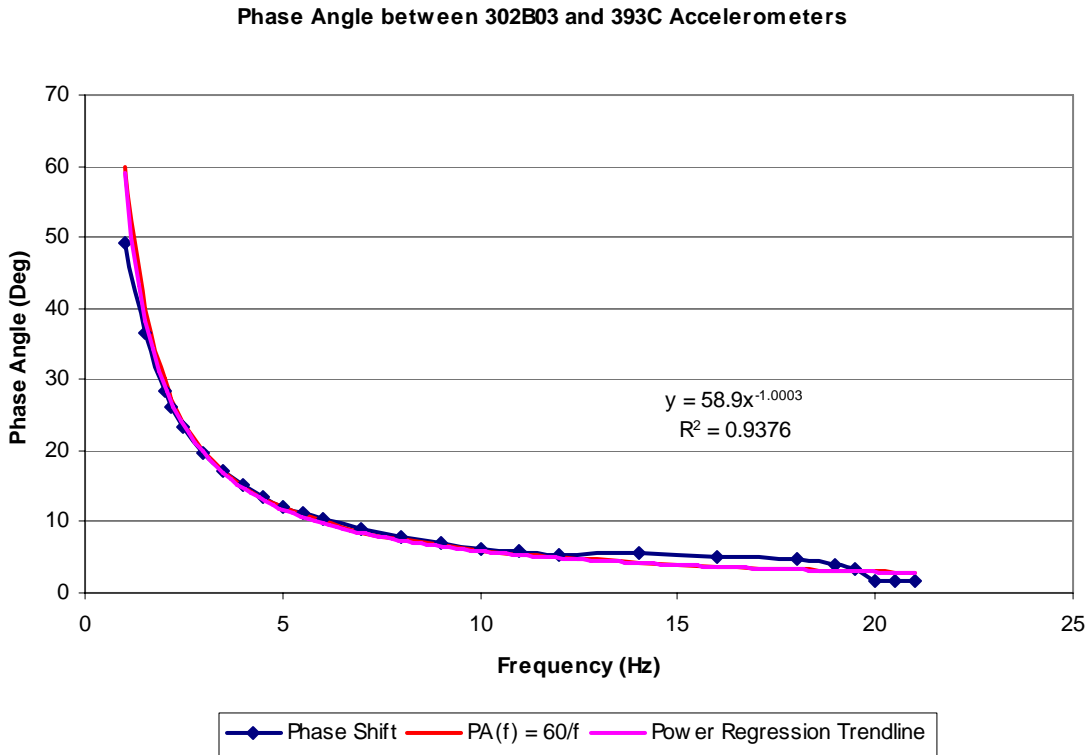


**Figure 5. Accelerometer Phase Angle Shift**

Both accelerometers have a 10-32 coaxial cable port built into them. A general-purpose cable assembly has the matching 10-32 plug at one end and a BNC plug on its other end to connect to a Sensor Signal Conditioner, more commonly referred to as a Battery Pack. The 10-32 coaxial connectors – commonly referred to as “submin” connectors – proved to be very

troublesome and were tested extensively before each trip, as well as with a multi-meter on site to ensure that the connections were functioning properly. The sub-min to BNC cables limited the approach to the field studies, as there were only a dozen available that functioned properly.

PCB model 480DO9 Power Units, commonly referred to as “battery packs,” provided excitation power in the form of a constant-current regulated, DC voltage source. Each battery pack requires three 9-volt batteries. The power units include optional gain settings of one, ten or one hundred. Because of the small vibrations encountered during the field studies, the highest gain setting was usually required. Each battery pack features a gage that shows the status of the batteries. During the field studies, these units had to be frequently checked to ensure that the batteries had enough power to drive the accelerometers. The 393C accelerometers in particular appeared to place a heavy drain on the power units and could cause even new batteries to have to be changed during an extended period of testing. The battery packs transferred the signal to the data acquisition system using a BNC to BNC cable. This project uses cable lengths that vary from 10-feet to 100-feet, depending on the location of the accelerometer on the bridge. Each BNC cable was tested with a multi-meter to ensure that they were functioning properly, and while the shorter wires showed negligible resistance, the longer wires consistently displayed a resistance of approximately one-one hundredth their length, in ohms. However, this level of resistance is considered acceptable for this project.

### **The Electrodynamic Shaker**

One effective way to identify the natural frequencies and their corresponding mode shapes is to excite the bridge at specific frequencies to locate resonances. This can be accomplished by introducing a controlled sinusoidal excitation using what is commonly referred to as a “shaker.” The current project used an Electro-Seis Electrodynamic Shaker, model 400-4012, made by APS Dynamics, and features a 100-pound auxiliary-reaction mass assembly of four attachable block masses during a portion of the studies.

The shaker is driven by the Dual-Mode Power Amplifier Model 144. During the tests, the amplifier was controlled by the Ono Sokki signal analyzer, which established the frequency and power level at which the shaker was driven. The force generated by the electro-dynamic shaker is proportional to the applied current. According to the product website, the shaker uses magnets configured such that the armature wire coil remains in a uniform magnetic field throughout the entire stroke, assuring force linearity.

At least one limiting factor must be considered in using a reaction mass shaker to drive a bridge structure. Assuming a reaction mass  $m$ , the force,  $F$ , generated by a reaction mass shaker moving harmonically through a displacement amplitude of  $u_0$  at frequency of  $f$  Hz is

$$F = 4\pi^2 f^2 m u_0 \quad [1]$$

Equation [1] contains three important factors:  $m$  and  $u_0$  are limited by the size of the available shaker, and by the available driving amplifier.  $f^2$  is the frequency that is to be excited, and is

determined by the natural frequencies of the structure. Most important, at low natural frequencies, the factor  $f^2$  is relatively small, so either a very large displacement amplitude  $u_0$  or a large reaction mass  $m$  is required to generate a significant force. By comparison, for large natural frequencies,  $f^2$  grows rapidly, and only a relatively small displacement amplitude  $u_0$  and reaction mass  $m$  is needed to generate substantial forcing. Since the lowest frequencies of the structure are often the frequencies of greatest interest, the ability of the shaker to drive these frequencies was uncertain prior to field testing. Excellent success was achieved using the shaker on the Wolf Creek Bridge, but this problem could also present itself in future bridge tests, especially if more massive longer span bridges, with lower fundamental frequencies are studied. Additional problems with shaker-structure interaction near resonance have also been noted in the literature (McConnell, 1995).

## **Data Acquisition Equipment**

### *Ono Sokki Signal Analyzer*

An Ono Sokki CF-350 Portable Dual-Channel Signal Analyzer was used throughout the project. Its first function was to allow the reading of real time data signals as well as to perform real time Fast Fourier Transform (FFT) analysis while on site at the bridge. During forced vibration studies, the FFT analyzer was especially useful for determining when the shaker had reached one of the bridge's natural frequencies. In addition, it allowed on-site reading of transform data from a vehicular or impulse excitation, providing information as to which frequencies should be excitable by the shaker. During the first trip to the bridge the FFT analyzer was used exclusively to identify not only whether or not the bridge could be excited adequately by the shaker, but also the frequencies at which it should be driven for full recordings at a later date. The second function performed by the signal analyzer was to control the frequency and power input to the shaker.

### *Campbell Scientific PC-9000*

The data acquisition system used in the first portion of this project was a Campbell Scientific CR-9000 Measurement and Control System and the PC-9000 Programming Software. Using two 9050 Analog Input Modules, the CR-9000 has the capability for 28 differential inputs to measure voltages up to 5-Volts in amplitude. The system incorporates a Sample and Hold feature that enables all of the signals to be recorded without any artificial phase shift between them. An important limitation of this system is that the 9050 modules available for the study do not have built-in filtering capability, although they do permit data integration before digitizing, so considerable care had to be taken to ensure that aliasing did not occur.

The PC-9000 programming includes a program generator as well as a more direct BASIC-style program editor option. For the relatively straightforward data acquisition needs of this project and possibly due to the forced nature of the vibration data, some features of the programming system proved to be more of a burden than an asset and caused several delays in the field.

## *MegaDAC 3200 Data Acquisition System*

A MegaDAC 3200 data acquisition system was used as a replacement for the PC-9000 when that unit became unavailable. The MegaDAC system has 28 differential input channels and like the PC-9000, its programming includes a Sample and Hold capability. Unlike the PC-9000, the MegaDAC system's data acquisition channels have built-in, software selectable 8 pole Butterworth filters, which makes the system ideally suited for recording dynamic data.

The MegaDAC computer interface is somewhat antiquated, consisting of a 1995 era Toshiba laptop running DOS 3. However, the MegaDAC operating system allows the user to view the real time signals of every channel simultaneously. A benefit of viewing the dynamic data in real time is that a malfunctioning transducer can be identified and repaired in the field. The MegaDAC system also allows data to be transferred directly to the host PC during sampling, expediting the testing process.

## **System Preparation and Data Retrieval**

### *Equipment Testing*

In preparation for the field tests, the equipment was subjected to a number of preliminary checks before being deployed on the bridge. All of the connector cables were checked with a multi-meter to verify the adequacy of the wire and connections. Next the cables and accelerometers were cross checked in various combinations in order to validate the signals produced by both the individual accelerometers and the power packs and the wiring.

The remaining accelerometers were attached directly to the shaker and connected to the signal analyzer to compare both the different types of accelerometers, and check each individual accelerometer's signals under known sinusoidal motion. The accelerometers were checked for any systematic errors in the signals, by subjecting them to a range of sinusoidal excitation frequencies from 1 to 20 Hz. The temporal signals were checked visually, and the transform amplitudes and phase angles were compared for consistency. Several of the accelerometers initially displayed very asymmetrical signals when excited at a frequency of around 1 Hz, and this was reflected by multiple peaks in the transformed signal amplitude as well. In a surprising development, several of the accelerometers that had not been used for some time as well as a few that had been considered malfunctioning by previous researchers were found to work very well once they had been excited through the full range of frequencies. The asymmetry of the time signals disappeared, even when the excitation frequency was decreased to the original 1 Hz. This "exercising" of the accelerometers seemed to correct any abnormalities in the signals. Subsequently, the accelerometers were put through these "exercises" a few days prior to any trip so as to help keep them in proper working order.

### *Methods of Excitation*

Three primary methods of exciting the bridge were utilized in the present study. This bridge is small enough and sparsely traveled enough that forms of both vehicular and controlled inputs could be used. Also, because of the low traffic volume, at least two recordings of every

type of excitation were made for all accelerometer positions. This helped to offset random noise effects during the data analysis.

The only method of measured input used was the shaker, and even then the only input measurement that is of any concern to this paper was the driving frequency itself. Force amplitudes were not measured. Using the shaker with the signal analyzer, the bridge was driven through the full frequency range of interest – that is 0-Hz to 30-Hz – and data recordings were taken when a natural frequency appeared to have been excited, as indicated by the response shown by the accelerometers connected to the signal analyzer. The shaker was placed halfway between the quarter-point and the mid-point on the outside curve of the center span in order to excite as many different modes as possible. Ideally the shaker would be moved to different locations on the bridge to excite different modes, but its weight, together with the difficulty in relocating the amplifier and the signal analyzer made that approach difficult and inefficient.

The second method of controlled excitation was a simple impulse generated by hitting the bridge in any number of ways, which allowed the bridge to vibrate almost completely free of any non-negligible weight or other noises. The impulses used were not measured, so it was not possible to back out either impulse response or transfer function information, but they generated very clean transient signals. The use of several reference accelerometers made it possible to extract mode shapes in this manner.

Quasi-ambient vibrations were created in two different ways. Initially a large dump truck was scheduled to be driven across the bridge at as high a speed as the drivers felt was safe. The truck was driven onto the bridge from each side so that both sides of the bridge were equally affected by any disturbance the truck's mass or speed may have on altering the vibrations while on the bridge. Ideally, the transforms would only be performed on the transient signal die out, after the truck has left the bridge entirely, but the amount of damping and slow vehicular speed in crossing the bridge made it difficult to achieve useful transient signals in this manner. Similarly, driving a minivan across the bridge created quasi-ambient excitations. Using the lighter, more maneuverable vehicle enabled somewhat higher speeds to be attained by the driver, allowing for a cleaner, though lower amplitude transient signal than the dump truck.

### **Placement of Accelerometers**

Since the primary objective of this project was to measure as many natural frequencies and mode shapes of the bridge as possible for comparison with the FE model, the layout of the accelerometers was of considerable importance. Ideally, the denser the array of accelerometers that can be used, the more completely the mode shapes can be characterized. Following the equipment check out, it was discovered that no more than 12 accelerometers could be deployed at one time. Given this limitation, a somewhat less ambitious instrumentation plan was designed.

Using the finite element analysis as a rough guide, locations that seem to be consistent with modal identification are the three midspans, six quarterspans, and directly above the piers on both the exterior and interior edges. A denser array is ideal, but not practical for this project, given the equipment limitations. The mid-spans would provide the maximum amplitude of single curvature symmetrical modes; the quarterspans would provide nearly maximum amplitude for

the double curvature modes; and the two sets would be out of phase with each other on third-order curvatures. It is also important to obtain data for the locations directly above the piers, since a major consideration of Lydzinski's study was determining whether representing the piers as simple pinned supports introduced significant errors into the dynamic analysis. Measuring radial motion of the bridge is also important, since this motion is one of the distinguishing response characteristics of a curved multi-girder bridge. The finite element models suggest that there is very little low-frequency, reversed radial motion within a single span of the bridge, so quarter span, radially-aligned accelerometers did not appear to be important, except for helping to provide smoother mode shapes.

It was not anticipated that the bridge would be closed to traffic, so it was generally only feasible to place accelerometers along the edges of the bridge for most of the studies, permitting both traffic lanes to remain open. Following the reasoning based upon the FE model, if similar accelerometer layouts were utilized on all three spans, a total of twenty-seven accelerometer locations, twenty-two vertically aligned accelerometers and five radially aligned, would be required. Additional accelerometers could then be used in the middle of the bridge deck to verify the existence of the transverse bending modes.

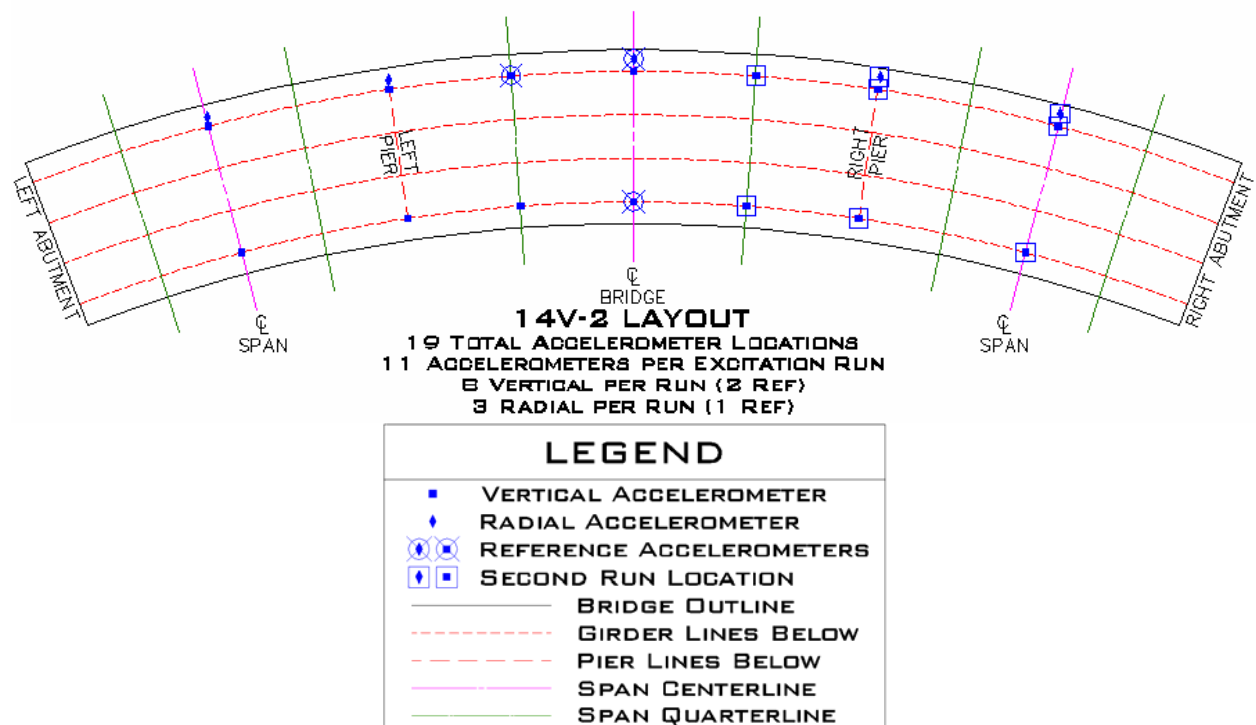
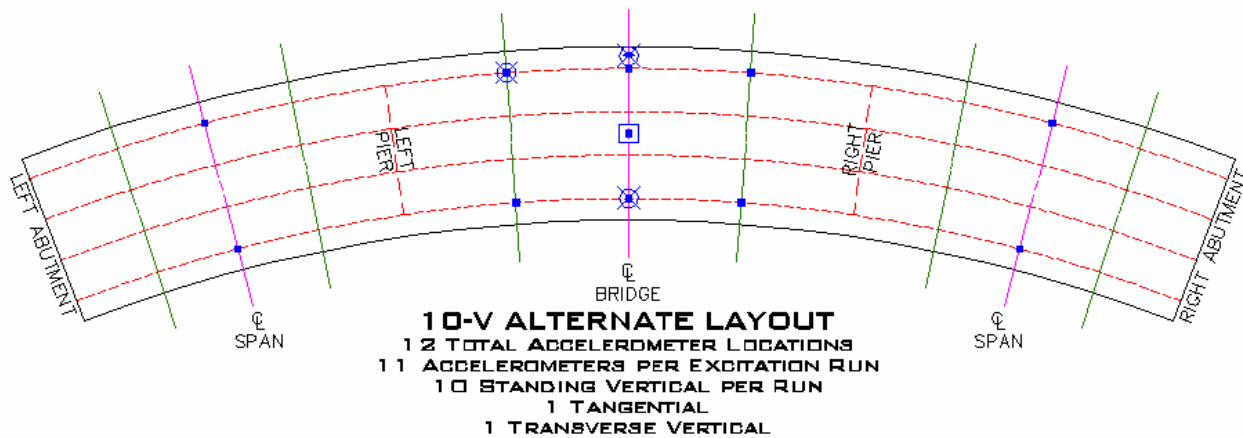


Figure 6. Fourteen V2 Accelerometer Layout

Once it was determined that only twelve fully functional accelerometer sets were available, Placing accelerometers at all 27 locations was not considered further. Based upon the initial finite element model, it was concluded that the quarter span locations on the end spans were probably unnecessary, since there did not appear to be any reverse curvature bending happening in the end spans within the frequency range of interest. Removing those 8 locations left only nineteen locations of interest, and only fourteen vertically aligned points. Following the preliminary laboratory tests, it was concluded that no more than 12 accelerometers would be

available at any time. Consequently, two separate setups were made per excitation type in order to obtain modal data for the entire bridge, and three reference accelerometers, shown in Figure 6, were used in order to properly compare the motions from each side of the bridge to the other.

During a planned trip to the bridge, the points shown in Figure 6 were instrumented in two setups, with three reference accelerometers. The initial setup instrumented the left half of the bridge, and the second setup instrumented the right half of the bridge, with the three reference accelerometers active in both setups. The data obtained from this study were very useful in identifying a number of natural frequencies and mode shapes. Unfortunately, several of the key accelerometers malfunctioned, a point that was difficult to determine in the field using the Campbell Scientific data acquisition system without extensive post-processing of the data. Therefore, a second trip was planned using a reduced set of accelerometers to fill in the missing data.



**Figure 7. 10-V Alt. Accelerometer Layout (Refer to Legend from Figure 6)**

Having already gathered useful data for the piers and radial direction under both forced and ambient excitations, it was decided to omit those nine locations from the layout of the bridge during the final trip. Also, since the trip's focus was placed on gathering end span modal data – specifically the direct phase difference between the two opposite ends – as well as longitudinal data and transverse bending data, only twelve accelerometer locations were needed, allowing for all excitations to be completed without rearranging the majority of the accelerometers, as shown in Figure 7.

Altogether, accelerometers were located at twenty-one different positions on this bridge. For organizational purposes in the field and later references in this paper, a simple set of four-letter labels was created involving the four types of distinctions that identify each position. The first letter refers to the curve of the bridge it is located on, that is the *Inner*, *Outer*, or *Middle* curve; the second refers to the span or pier: *Left*, *Center* or *Right*; the third tells whether the signal is generated at the *Mid-span*, *Left quarter span*, *Right quarter span*, or *Pier*; and the last letter denotes whether the accelerometer is *Vertically* aligned, *Horizontally* (radially) aligned, or *Longitudinally* (tangentially) aligned. A full list of the different positions is given in Table 2.

**Table 2. Accelerometer Position Labels**

Label	Position	Label	Position
OLMV	Vertical, Outside Left end Midspan	ICRV	Vertical Inside Center Right Quarterspan
OLPV	Vertical, Outside Left Pier	IRPV	Vertical, Inside Right Pier
OCLV	Vertical, Outside Center Left Midspan	IRMV	Vertical, Inside Right end Midspan
OCMV	Vertical, Outside Center Midspan	OLMH	Radial, Outside Left end Midspan
OCRV	Vertical, Outside Center Right Quarterspan	OLPH	Radial, Outside Left Pier
ORPV	Vertical, Outside Right Pier	OCMH	Radial, Outside Center Midspan
ORMV	Vertical, Outside Right end Midspan	ORPH	Radial, Outside Right Pier
ILMV	Vertical, Inside Left end Midspan	ORMH	Radial, Outside Right end Midspan
ILPV	Vertical, Inside Left Pier	OCML	Tangential, Outside Center Midspan
ICLV	Vertical, Inside Center Left Quarterspan	MCMV	Vertical, Middle Center Midspan
ICMV	Vertical, Inside Center Midspan		

*Executing the Field Studies*

Four trips to the Wolf Creek Bridge were made over about a six-month period, an initial exploratory trip, in which preliminary data were gathered, and three trips to gather the detailed accelerometer data to construct mode shapes.

The first trip to the bridge had two major objectives. The first objective was to determine whether the available Electro-Seis shaker could generate adequate response signals to permit good data to be obtained. The second objective was to obtain preliminary frequency estimates using only a limited number of accelerometers in order to expedite the testing when the full array of accelerometers was deployed subsequently. For this trip, only the signal analyzer and two accelerometers were used. The two accelerometers were placed at the mid-point and quarter-point of the exterior center span and the shaker was placed vertically, midway between them with the intent of exciting both symmetric and anti-symmetric modes. The signal analyzer was then used to generate harmonic excitation, beginning at one Hz, and gradually increasing, until a region of near resonance was found. At this point, smaller frequency increments were used in the vicinity of the resonant peak to isolate the natural frequency. The frequency stepping was then continued up to 30 Hz. This procedure provided a set of frequencies to focus upon during the following trips to the bridge with the full array of accelerometers. It was found that the bridge was actually quite easy to shake using harmonic excitation, and eight frequencies were noted which were to be excited on the following trip: 2.3-Hz, 3.2-Hz, 4.4-Hz, 6.9-Hz, 8.6-Hz, 12.4-Hz, 14.5-Hz, and 24.5-Hz.

After cycling through the 30-Hz range a second time, the shaker was then laid down in the radial direction and the 393C accelerometers were replaced with 302B03 accelerometers. Unfortunately, in laying the shaker on its side, two of the weights had to be removed in order to clear the ground. The shaker was still able to lock into two frequencies, 5.25-Hz and 6.9-Hz, showing that at least one mode combined vertical and radial motion as was expected, given the curved nature of the bridge. However, the shaker was not able to excite the first mode predicted by Lydzinski’s finite element analysis when radially oriented.

The second trip to the bridge on November 9, 2006 was generally unsuccessful, because a painting crew with a heavy snooper truck was present during the entire day. Although six data sets were recorded, the files were discarded because of the poor data quality.

The third trip to the bridge on December 11, 2006 produced generally good data. The accelerometers were located on one half of the bridge at a time, following the 14V-2 setup shown in Figure 6. An extra accelerometer setup was deployed to allow the entire exterior, center span to be present for every record. Starting out with the accelerometers on the left side of the bridge, the shaker locked into five of the nine frequencies that had been found on the first trip, and one more that had not. However, for reasons not fully understood at the time, none of the frequencies excited were exactly the same as those found during the first trip and the two lowest frequencies obtained during the first trip (2.3 Hz and 3.2 Hz) could not be found at all. 4.6-Hz was by far the strongest recorded signal and a signal at 12.12-Hz was the second strongest, but signals were also recorded at 5.20-Hz, 5.27-Hz, 6.36-Hz, 6.61-Hz, 10.23-Hz, and 24.00-Hz.

As a somewhat naïve experiment, a recording was started just before creating a single, unmeasured impulse. The impulse reaction was so strong on the signal analyzer that it was decided that to record several impulse responses. The single impulse excitations provided the cleanest data obtained during the trip. Based upon this observation it was decided that impulse loadings would be a primary means of excitation if additional data were needed.

The third trip also produced several vehicular excitations, mostly by a moderate sized Honda minivan, but two specific runs by very heavy logging trucks, all of which turned out to be very enlightening in this project. The heavy trucks were not able to drive over the bridge at more than 10-miles per hour, and therefore the excitations were not very clean and the frequency data were probably influenced by the weight of the truck itself. By comparison, the van was able to excite the bridge satisfactorily as well as exit the bridge quickly enough so as not to greatly affect the natural frequency response of the bridge. However, it should not be inferred that such a small vehicle would be a good excitation for larger structures, where higher vehicular velocities are possible.

During the third trip, two of the key accelerometers (OCMV in particular) did not function properly. Although the source of the malfunction was not precisely identified, the most likely source of the malfunction was the subminiature connectors, which had previously been found to be troublesome. Whatever the reason, the accelerometer on the exterior, center mid-span did not produce viable data. Several other accelerometers produced a skewed signal, but in those cases the data were still adequate to produce reasonably accurate transforms, though there was a substantial frequency-domain response at frequencies below 1-Hz in those data.

Although the data from the third trip produced strong, clean mode shapes, the exterior, center mid-span is an important data point on the bridge and although the shape could generally be predicted by the radial and quarter span motion, the modal data were considered incomplete. Continued analysis of the computer models raised questions about movement in directions that had not been monitored before that could only be addressed by placing one or more accelerometers midway across the bridge surface. Moreover, it was realized that the most

significant motion at the 2.3-Hz frequency was in the tangential direction, and no previous attempts had been made to excite the bridge in this direction, nor had any tangentially oriented accelerometers been used.

To fill in the missing data, and to address the questions about the missing modes, a final trip to the bridge was planned on March 20, 2007. Believing there were sufficient data from the pier locations and radial aligned accelerometers, it was decided to use the symmetrical, 10-V setup as discussed above. In addition, an eleventh accelerometer was set up to be aligned first in the tangential direction at the exterior center mid-span, and later vertically along the centerline of the bridge at center mid-span. The reduced number of accelerometers used during this trip also allowed both end spans to be recorded at the same time so as to determine their relative phase angles in relation to each other, specifically on the mode shapes that featured little to no center span motion. The bridge was struck with impulses from five locations on the bridge. Two vertical impulses were applied at the exterior and interior center mid-span, the left exterior center quarter-span, and both of the exterior end spans, providing ten data records to aid in building mode shapes. Two tangential impulses were planned after that. Three additional impulse responses were recorded from the left exterior center quarter-span with the accelerometer in the middle of the bridge to record transverse motion, and four van runs were made with the eleventh accelerometer off to the side.

## Data Analysis

### *Transform Analysis and Modal Identification Strategy*

The natural frequencies and information about the mode shapes were extracted for this project using a frequency domain peak picking approach. Other algorithms exist in both the time and frequency domain (See Maia et al (1997), for example.) but were not utilized in the current study, since the primary objectives of validating the FE model and gaining insight into the behavior of the bridge were adequately addressed using the more straightforward approach. The time domain data files were first transformed into the frequency domain using the FFT, a widely used algorithm that efficiently calculates the discrete Fourier transform (DFT)

$$S\left(\frac{n}{NT}\right) = \sum_{k=0}^{N-1} s(kT)e^{-j2\pi nk/N} \quad n = 0, 1, \dots, N-1 \quad [2]$$

Equation [2] transforms the time function  $s(kT)$  sampled at uniformly spaced time intervals  $T$ , into the complex frequency spectrum  $S(n/NT)$  at uniform frequency increments  $n/NT$ . The advantage of the FFT algorithm in evaluating eqn. [2] is purely computational, but the time savings is considerable. Readers are referred to Brigham (1988) or McConnell (1995) for details.

Following transformation of the measured signals into the frequency domain, the resulting complex frequency spectra were then converted into amplitude and phase angle spectra. The peaks of the frequency amplitude spectra were identified, and used to estimate the natural frequencies of the bridge. The amplitudes of vibration in the different modes were then extracted from the peak amplitudes, and scaled relative to the reference accelerometer amplitudes. In addition, cross-spectra were constructed between the reference accelerometers, and the

remaining accelerometers, and the resulting phase angles were used to estimate whether signals are in phase or out of phase. Generally, this approach works adequately for bridge structures, which are lightly damped, so phase angles tend to be either near zero or  $\pm 180^\circ$ .

Equation [2] reveals one aspect of the DFT that is essential in the decision making process concerning the length of time sampled. The final frequency function  $S$  is evaluated only at discrete frequency steps  $1/(NT)$ , so the frequency resolution is limited by the length,  $NT$ , of the sample record in the time domain. For example, a response sampled at an interval of  $T$  seconds for a total of 10 seconds will only be able to produce a frequency resolution of  $1/(10 \text{ seconds}) = 0.1 \text{ Hz}$ , while sampling for a total of 50 seconds would produce a frequency resolution of  $1/(50 \text{ seconds}) = 0.02 \text{ Hz}$ . The difficulty encountered in field testing is that it may not be possible to obtain a meaningful response record of 50 seconds duration, depending upon the source and amplitude of the excitation. For example, the useful signals obtained from impulse loadings on the current bridge were only about 15-20 seconds long. Hence, the ability to resolve frequencies precisely using free vibration response may be limited practically.

The sampling rate also significantly influences the computed results. This is not obvious from eqn. [2] but has been explored thoroughly in the literature. If the highest frequency present in the signal is  $f_{\max}$  Hz, a maximum sampling rate no smaller than  $f_{\text{Nyquist}} = 2f_{\max}$  is needed. This sampling rate, known as the Nyquist rate, is necessary to avoid a phenomenon called aliasing in which higher frequency signals are indistinguishable from lower frequency signals. Convolution overlap occurs until the separation of the frequency impulses is increased to twice that of the largest frequency present in the signal. Several additional complications may also arise. If  $f_i$  is the highest frequency of interest in the signal, but higher frequencies up to  $f_{\max} > f_i$  are also present, then the sampling rate must be based upon the frequency  $f_{\max}$ , and not on  $f_i$ . A common solution is to filter the higher frequencies out of the data before sampling. As noted above, the MegaDAC system's channels have this capability, but the PC-9000 system channels do not. Therefore, considerable care had to be used when employing the PC-9000 to sample at a rate controlled by the highest frequency observed in the signal.

### *Preliminary Studies and Software Development*

Once the acceleration data were recorded by the data acquisition systems, the data files then had to be analyzed. Because of the large amount of data, a number of MATLAB M-files were generated to transform the raw data from the field tests. For a full list of the MATLAB user-defined functions developed for this project, see Turnage (2007). Two preliminary studies were carried out to evaluate the MATLAB modules.

1. To become more acclimated with MATLAB programming as well as the programming of the PC-9000, a simple three-story frame model was set up to serve as an initial test for the MATLAB and PC-9000 software. This structure allowed the researchers to focus on programming the data acquisition system and the transform functions, and using this model, the PC-9000 recording program was written as well as MATLAB functions to retrieve the ASCII files and transform the data in a systematic manner.

2. To replicate the expected modal interference from closely spaced modes, a series of artificial data files, whose frequencies were selected based upon Lydzinski's flexible pier model and whose amplitudes were adjusted to create potential problems were evaluated using the MATLAB modules.

See Turnage (2007) for additional details on these studies. The MATLAB modules performed satisfactorily in both of these preliminary tests, so they were employed to systematically analyze the field data.

### *Accumulating Mode Shapes*

The FFT algorithm in MATLAB was used to transform the data from the various data files into the frequency domain. Then, the amplitude and phase spectra were constructed in preparation for modal identification. The MATLAB modules written for this project were then utilized to locate the natural frequencies from the transformed frequency domain data. Once the natural frequencies were picked, it was necessary to organize the amplitude and phase angle data into mode shapes. Several things complicated this process. The same data that demonstrated the percent errors in the frequency in the previous section also showed that in some cases this error causes two slightly different frequencies to be picked for the same mode. While the actual frequencies were known in the case of the artificial data, the same is not true for the field data, and with the models predicting that several pairs of natural frequencies are closely spaced; it is not possible to know which mode each frequency belongs to without comparing the shapes.

Therefore, the first organizational function for MATLAB to perform was to take the natural frequencies from each signal and graph a mode shape from them. While doing this for a few, linearly arranged signals, or even a two dimensional array of points on a straight bridge is very simple, doing this for a two-dimensional, curved roadway is not. After several trials, it was concluded that a three-dimensional wire frame representation of the data was overly confusing because of the bridge's curvature, so the mode shapes were organized by position along the bridge centerline and exported into two-dimensional graphs generated by EXCEL with separate series for the exterior vertical motion, the interior vertical motion, and the radial motion. These graphs allow the identified frequencies to be categorized into the correct mode shape group for averaging.

Once the range for the individual modes were identified and a frequency range was established for the modes, MATLAB then imported them back and accumulated them into one large file for averaging. Similarly, the individually identified frequencies from the Fast Fourier Transform data can also be grouped and averaged as well. To further understand the bridge, another function separated out all the frequency domain data by their location, to see how the different excitation methods affect the different modes.

# RESULTS

## Identified Frequencies and Mode Shapes

### First Mode: 4.565-Hz

The strongest mode observed was the first bending/torsion mode, found at about 4.56-Hz. This frequency was picked up on virtually every recording, including several recordings while the shaker was attempting to excite a different frequency. The vertical motion in this mode was visible by the naked eye when the motion was driven by the shaker. The data indicate that vertical motion of the bridge is dominated by motion of the outside edge of the bridge, as is shown in Figure 8. Averaging the frequencies obtained from the various excitations gave a mean predicted natural frequency of 4.565-Hz with a standard deviation of 0.024-Hz. The frequencies predicted by the shaker-driven excitations tended to be slightly higher than those obtained from impulse excitations due to a moderate amount of interaction between the bridge and the shaker. Frequencies from the shaker were consistently found at 4.590-Hz, without exception, while the impulses and vans typically excited around 4.557-Hz and 4.573-Hz, respectively. The piers show a small amount of motion, and a small amount of bending occurs on the inside edge, but the mode is dominated by first-mode vibration of the outside edge, with the center span seeing the most movement. The data also indicate significant radial motion of the deck, predominantly on the center span. It appears almost as if the outer girders were using the piers as a pivot point, just as if it were a simply supported beam.

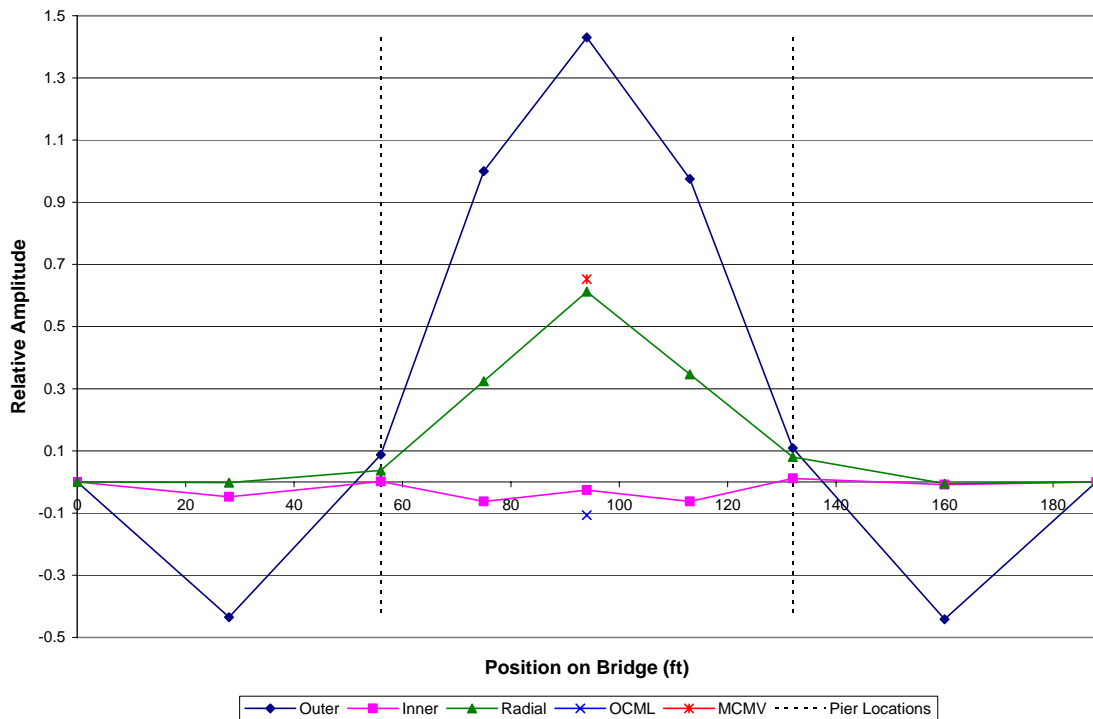


Figure 8. First Mode: 4.565 Hz/±0.024 Hz

## Second Mode: 5.215-Hz

The second mode is dominated by vertical displacement on the inside edge of the bridge center span as well as a significant amount of pier cap rotation and a small amount of radial displacement. Averaging the test data for this mode, including six specific runs of shaker excitations, showed a mean natural frequency of 5.215-Hz with a standard deviation of 0.049-Hz. The shaker excited this mode of the bridge at two slightly different frequencies, 5.20-Hz and 5.27-Hz. Both sets of data revealed the same relative displacements and phase angles, so both sets of data were averaged into the mode despite this incongruity. The second mode has a substantial out of phase motion on the outer edge of the bridge at about half the amplitude of the inside edge motion as shown in Figure 9. These combinations seem to suggest a mode dominated by inner edge bending, plus some overall twisting of the bridge girders and significant rotation of the pier caps about a tangential axis. The entire outer edge of the bridge is out of phase with the center span inner edge displacement while the inner edge of the end spans is out of phase with the center span, suggesting that while the outside edge is primarily vibrating up and down with the piers, the inside edge girder is undergoing a bending mode with reversal of curvature of the end span motion in addition to the observed pier motion.

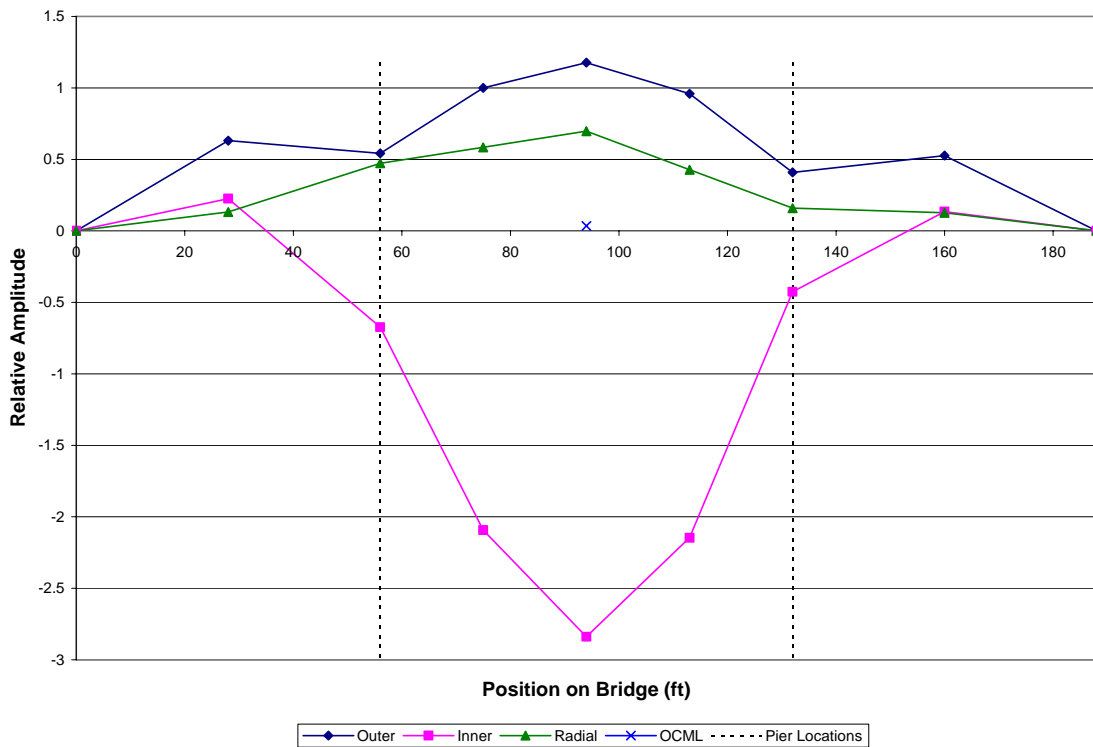


Figure 9. Second Mode: 5.215 Hz/ $\pm$ 0.049 Hz

## Third Mode: 6.500-Hz

The third mode presents what appears to be the first torsional mode of the bridge. The field data predict a mean natural frequency of 6.500-Hz with a standard deviation of 0.102-Hz, this mode produced the strongest vibrations on the inside curve of the bridge, under direct

impulse excitations, although the ninth mode produced stronger motion under regular vehicular loading. Only a small amount of pier rotation occurred in this mode, as shown in Figure 10. This is not surprising since the three spans tend to twist in alternating directions in this mode, so the piers would be expected to be very near the nodes of the motion. Twisting of the end spans appears to occur roughly about the longitudinal centerline of the bridge, but the center of twist in the center span appears to be somewhat closer to the outside girder, suggesting that some bending as well as twisting may be occurring on this span. The motion of the inside edge of the center span is about three and a half times that of the end spans.

**Fourth Mode: 7.396-Hz**

The identified fourth mode motion is anti-symmetrical, and largely concentrated in the two end spans. Beginning with this mode it became considerably more difficult to determine the exact shape of each mode as more of the frequencies not only combine bending and torsion motion, but also have more complicated longitudinal displacement profiles at frequencies that are not well separated from each other. A further complication for the modes that are dominated by end span motion was that having reference accelerometers near the center of the bridge for modes that typically did not have large center span motion meant that normalizing the motion for different runs proved highly inconsistent.

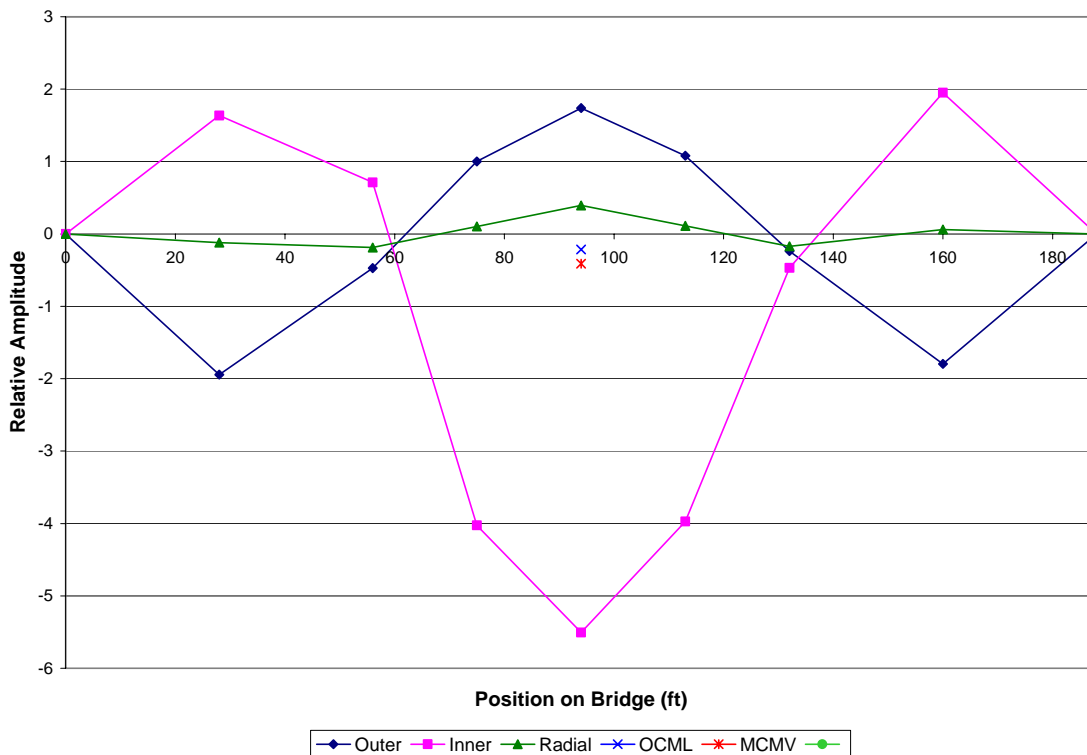


**Figure 10. Third Mode: 6.500Hz/±0.102 Hz**

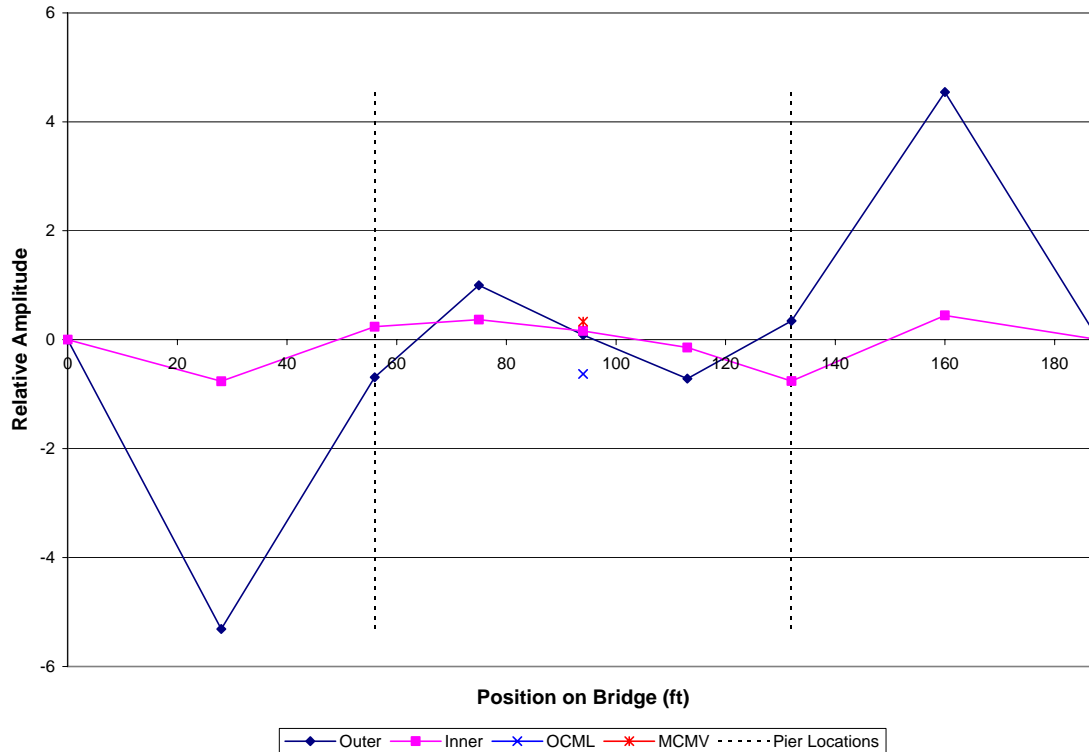


**Figure 11. Fourth Mode: 7.396 Hz ± 0.031 Hz**

Having a mean natural frequency of 7.396-Hz with a standard deviation of 0.031-Hz, based upon the field data, the fourth mode proved to be the mode with the largest exterior span motion along the outside edge of the bridge and possibly the second strongest mode on the entire bridge under ambient excitations. A fairly simple mode as Figure 11 shows, the majority of its motion is the out of phase vertical vibration of the two exterior spans along the outside curve of the bridge. The inner edges of the outer spans undergo significantly smaller displacements than the outer edges, but are in phase with the outer edges, suggesting that the predominant motion is end span bending, with a small amount of twist. There is also reasonably consistent motion on the bridge at this frequency as a seemingly second order bending along the outside curve of the center span appears to undergo a reversed curvature bending displacement, and the inner edge of the center span is largely in phase with the outer edge, except that the piers are out of phase. An impulse at the center, quarter span does not seem to excite the mode appreciably. Although the mode was known to exist prior to the final trip out to the bridge, the available data for this mode had been obtained by exciting the center span, so the amplitude of this mode was noticeably weaker than several other modes. In an attempt to improve the measured signals for this mode, and other modes with strong end span components, it was decided that the final trip should include several impulses applied on the end spans.

### **Fifth and Sixth Modes (8.715 Hz and 8.915 Hz)**

The next two modes provided a challenge in distinguishing the exact mode shapes, and showed the limitations of the peak picking algorithm in separating specific modes whose frequencies are close together. Both modes were fairly easy to spot at the specific locations of

largest displacement, but without using the shaker to specifically excite each of the two frequencies separately, the motion at those frequencies at all the other locations tended to be difficult to separate. Therefore, although the frequencies of modes 5 and 6 obtained from field data are reasonably accurate, the mode shapes are not equally good. Before considering the field data, it is useful to examine the mode shapes of the fifth and sixth modes predicted by the modified FE model. The FE model predicts that Mode 5 is symmetrical about middle of the center span, and is dominated by motion of the outside edge, while the inside edge of the bridge undergoes little motion in the fifth mode. By contrast, mode 6 is anti-symmetrical, and is largest on the inside edge, with relatively small motion on the outside edge of the bridge. Because of the closeness of the two frequencies, (8.715 Hz and 8.915 Hz in the modified FE model) it can be anticipated that a peak picking algorithm using the frequency domain data will encounter difficulty predicting the displacements on the inside edge for mode five, and on the outside edge for mode six.

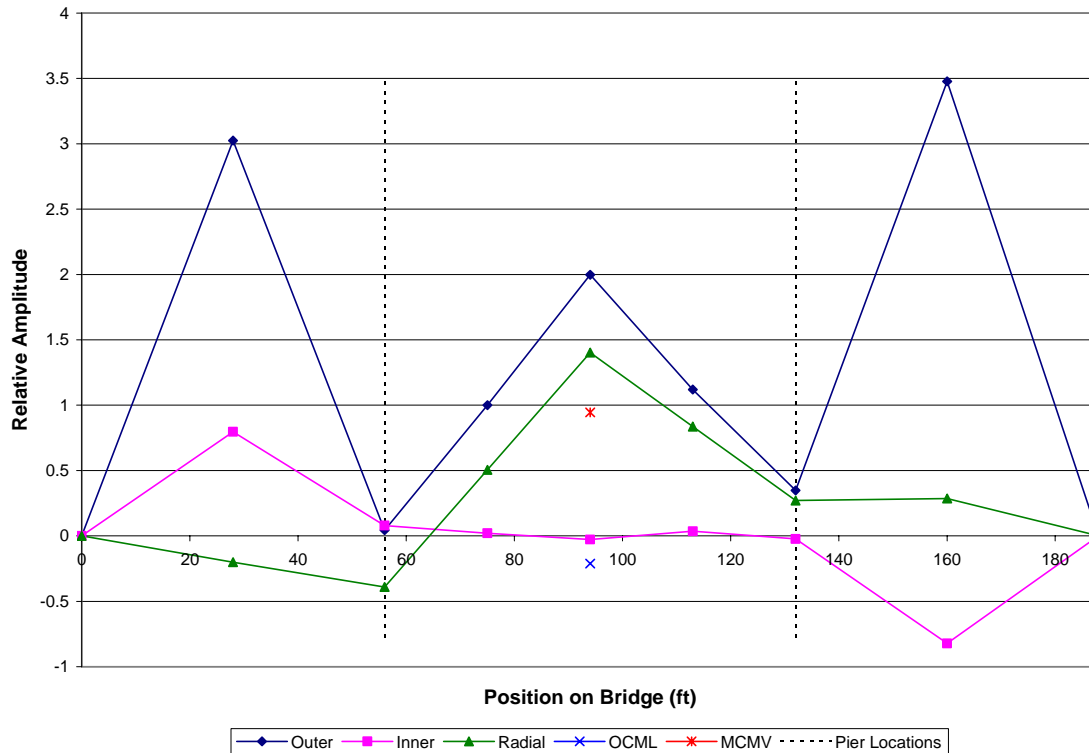


**Figure 12. Fifth and Sixth Modes: 8.730 Hz and 8.915 Hz**

The fifth mode displacements are dominated by vertical, almost symmetrical displacements of the outer edge, as shown in Figure 12. However the measured motion along the inner edge of the bridge appears to be nearly anti-symmetric. Given the nearly symmetrical nature of the structure, it appears that two modes are present at nearly the same frequency. The presence of two modes is further verified in comparison with the FE models, discussed later. Because of the proximity of the two frequencies it was difficult to extract the motion of mode six, although the inside edge motion shown in Figure 12 is probably a reasonable approximation. Likewise, the small anti-symmetric motion of the outer edge in mode 6 is difficult to extract directly, because it is dominated by the large outside edge symmetric motion of mode 5.

Accumulating the frequencies for the fifth mode as well as possible, the mean measured natural frequency is estimated to be 8.730 Hz, with a standard deviation of 0.094 Hz, although this value may be a little high due to the difficulties separating the two modes from each other. It is also worth noting that measurements obtained during the final trip to the bridge, when the end spans were directly excited, produced a significantly higher natural frequency than the third trip. While data obtained during the third trip only produced eleven frequency domain peaks that were attributed to these modes, the majority of them were decidedly lower than the rest of the frequencies, averaging a natural frequency of just 8.605 Hz and falling as low as 8.521 Hz, while the final trip producing a mean natural frequency of 8.753 Hz and a standard deviation of 0.72 Hz. Further scrutiny of these low-lying data points shows that the vast majority of them were obtained from the data sets obtained from the two heavy logging trucks that drove over the bridge at slow speeds. During this time the weight of the truck would have a significant impact on the system and likely lower most, if not all of the frequencies.

Unfortunately, because the side spans were only excited from the outer edge of the bridge and by vehicle runs, the sixth mode is dominated by the fifth, so identifying a precise frequency value for the sixth mode is difficult, as every mode shape that can be pinpointed always has just as many, if not more, characteristics in common with the fifth mode than the sixth. Looking directly at the frequency peaks from the interior side spans along with those that seem to appear to the side of the stronger fifth frequency and the ones that do not seem to quite fit into the range of the fifth frequency, the sixth mode appears to have a natural frequency of about 9.120-Hz with a standard deviation of 0.067-Hz. Those numbers should be taken with extreme caution though, as there were only nine peaks to average.

### **Seventh Mode: 10.188-Hz**

The seventh mode displays a similar symmetrical displacement pattern to mode 5, but is dominated by motion of the inside edge of the bridge. The data somewhat suffered from the fact that it was never directly excited, but it was always evident, even early on as the shaker was able to lock into it briefly, during the third trip to the bridge.

Accumulating the data and normalizing it to the interior, left end span, rather than the much smaller signal at the left-quarter, center span, gave a natural frequency of 10.188-Hz with a standard deviation of 0.073-Hz. As shown in Figure 13, the motion is dominated by in-phase vertical vibration on the inside edge of the side spans with a much smaller out of phase motion on the outer edge of the side spans, suggesting side span torsion and some in-phase vibration of both the inside and outside edges of the center span. It also appears that the vibration amplitude of the right end span is not as large as the left end span, sometimes as little as only half of the strength, which seems peculiar considering the symmetry of the bridge. Most of the data for this mode were obtained during the final trip where the excitation impulses were applied on both sides of the bridge, so it would seem that any asymmetry would average out with the excitations on the right half of the bridge exciting the right span just as much as the left side impulses excited the left span. However this was not the case. One possible explanation is that since this mode is located between two modes in which the inside edge of the end spans are out-of phase with each other, one side span receives a slight increase from the adjacent modes, while the other receives a slight decrease from the adjacent modes. If this is the case, a purely symmetrical

excitation applied at the inside edge of the center span mid point should reveal a symmetrical mode shape.

A further breakdown of the data also shows that the frequency predicted by the shaker data was again somewhat higher than the impulse data. While the shaker consistently locked into this modal frequency at 10.230-Hz, the impulse responses had a mean frequency of 10.146-Hz with a standard deviation of 0.066-Hz. The van data were, unsurprisingly, not nearly as consistent as either of those excitation methods, and excited frequencies both above and below the two other methods, but it did still predict an average frequency of 10.184-Hz, again somewhat lower than the shaker data.

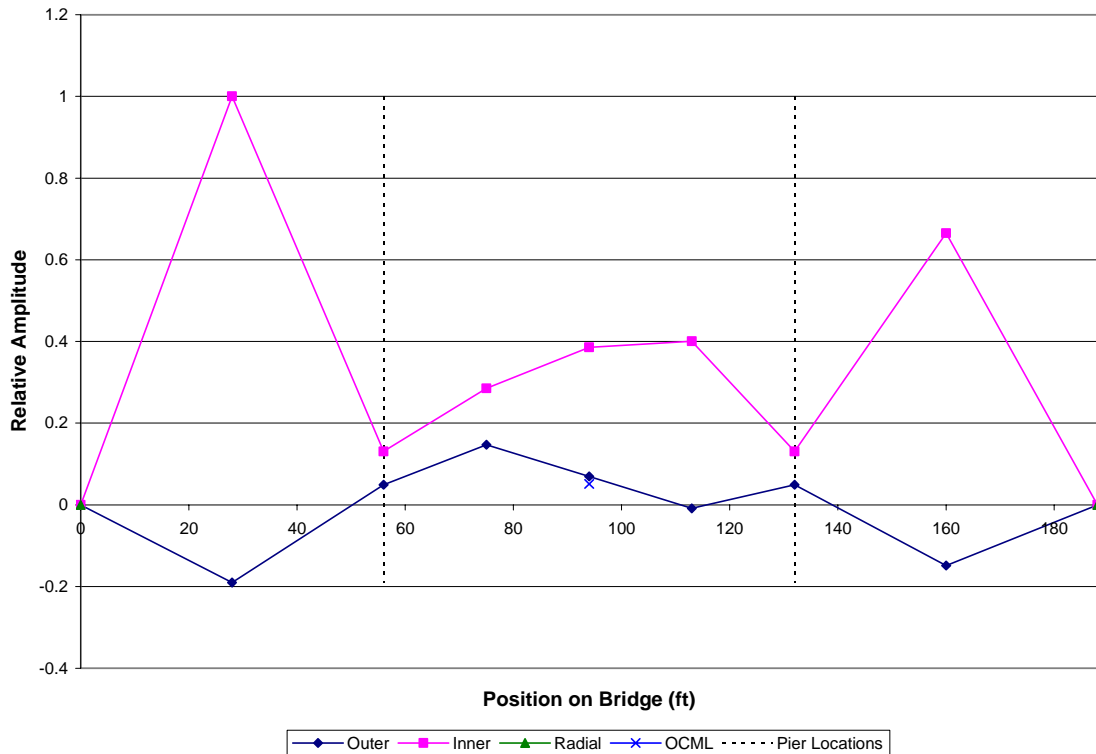


**Figure 13. Seventh Mode: 10.188-Hz ± 0.73 Hz**

### **Eighth Mode: 10.505-Hz**

Identifying the eighth mode led to many of the same difficulties associated with separating the fifth and sixth modes. This mode was originally thought to be erroneously accumulated data that was not consistent with any mode shape, with a mean measured natural frequency of 10.505-Hz and a standard deviation of 0.117-Hz. In fact, while the accumulated (averaged) data provide a fair approximation to the mode shape, no individual set of data appears to portray the expected shape very accurately. Mode 8 is the second mode displaying significant radial motion with a reversal of directions near the middle of the center span as well as apparently being the second torsional mode of the center span. As shown in Figure 14, the motion is approximately antisymmetrical about the longitudinal centerline of the road, and the

mid-span. The radial motion of this mode also shows that this mode probably includes the second radial vibration mode of the bridge and provides further evidence of the complexities caused by the curved nature of this type of bridge, and the flexible piers.

The data predict non-zero vertical motion at the mid-span, which is not expected, given the asymmetrical nature of the mode, but since the entire mode was never purposefully excited and the frequency is relatively close to the symmetrical mode 7, the results are reasonable.

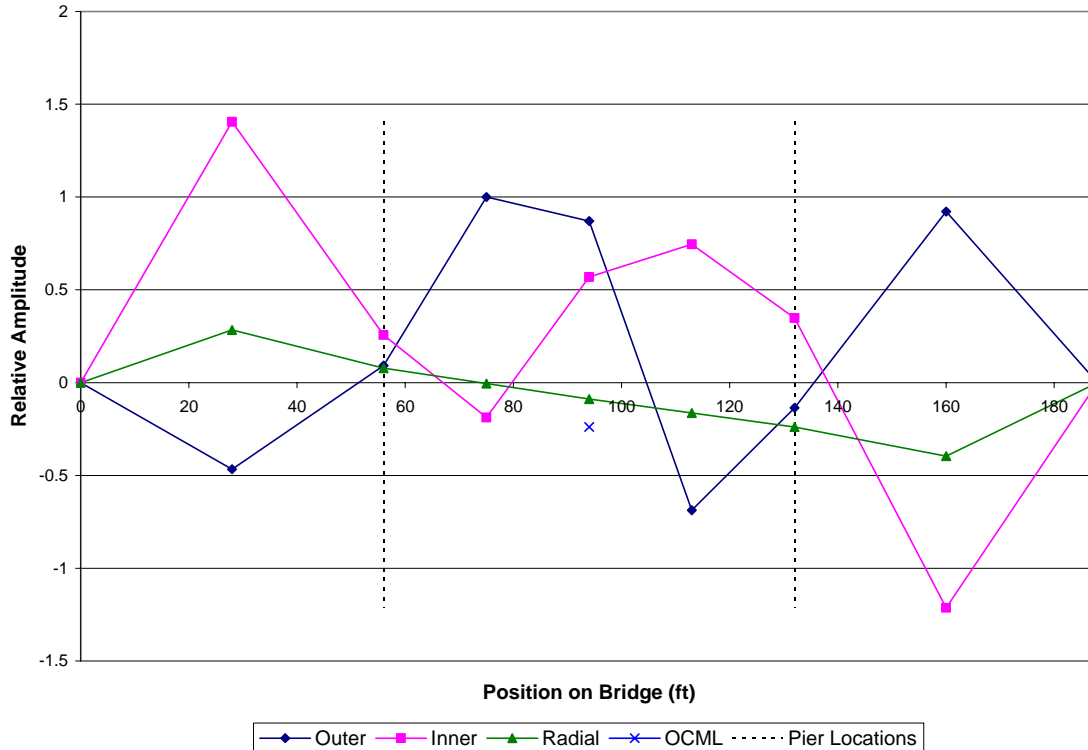


**Figure 14. Eighth Mode: 10.505 Hz±0.117 Hz**

### **Ninth Mode: 12.186-Hz**

The ninth mode introduces another form of vibratory motion into the bridge: transverse (sometimes called “hogging”) vibration. The ninth mode is either the third or fourth strongest mode on the entire bridge, with a particularly strong response to vehicular excitations.

Averaging the data indicates a natural frequency of 12.186-Hz with a standard deviation of 0.066-Hz. As shown in Figure 15, most of the vibration is confined to the center span interior and exterior edges being in-phase with each other and the end spans experiencing a smaller, out of phase motion. If only data from the inside and outside edges of the bridge are examined, the bridge appears to be experiencing a simple first order bending motion at each span. This appearance initially created some confusion as to why such a strong, simple mode did not seem to be shown in any of the finite element analyses. To verify that this is the first transverse mode, an accelerometer was placed in the middle of the bridge during the final instrumentation trip and showed that there was in fact a significant transverse bending motion at this frequency as the starred point on Figure 15 shows.

The FFT data show that this frequency was the strongest mode for particular locations under certain impulses. A somewhat minor discrepancy from the lower modes was that the shaker-induced vibrations obtained during the third trip tended to predict a lower frequency than those created via impulses and vehicular runs as well as those shaker-induced excitations from the second trip.

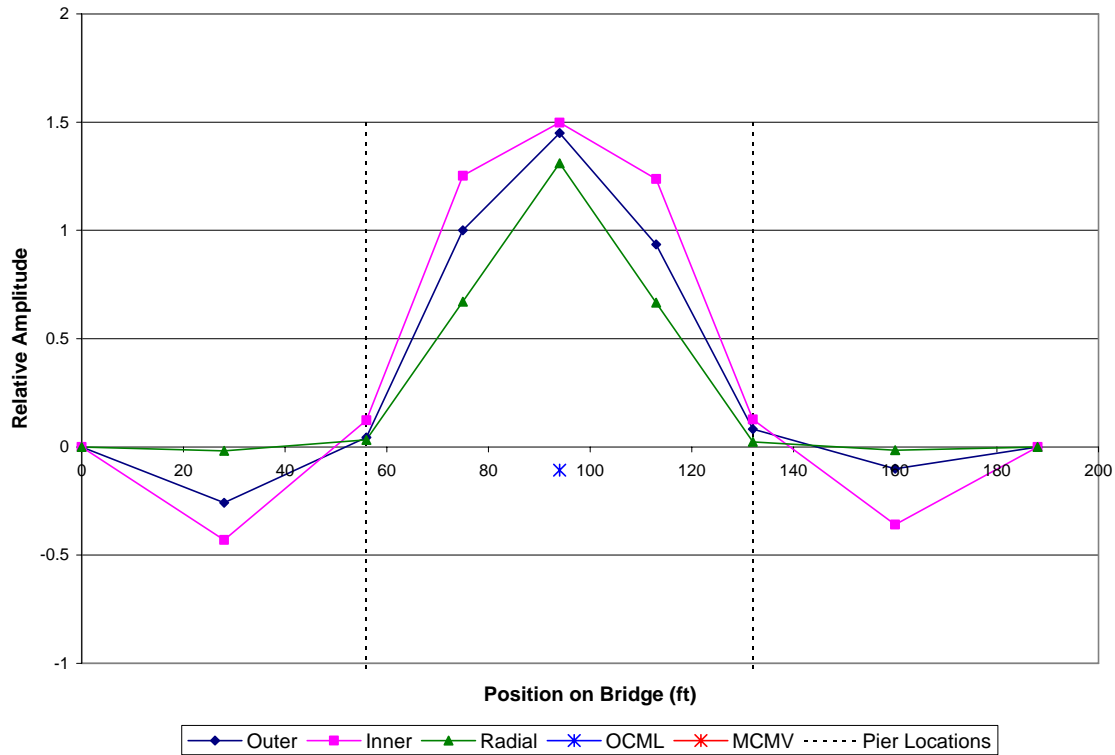


**Figure 15. Ninth Mode: 12.186 Hz ± 0.066 Hz**

Further complicating this discrepancy between the shaker driven and impulse excited data is that when the data are segregated according to the trip on which it was produced, there is almost no overlap in the nearly two hundred frequency calculations attributed to this mode. Taking the data from the third trip, it is noted that all ninety frequency estimates fall between 12.061-Hz and 12.183-Hz, and that, with just three exceptions, all one hundred and two frequency estimates found on the fourth trip were between 12.207-Hz and 12.305-Hz. The two separated sets of data produce means of 12.122-Hz and 12.242-Hz, with nearly identical standard deviations of 0.025-Hz and 0.028-Hz, respectively, both about equal to a single step in the frequency domain, while the differences between the two means are nearly ten times that.

### **Tenth Mode: 14.484-Hz**

The anti-symmetrical tenth mode appears to be the second bending/twisting mode of the outer edge of the center span. An extremely strong mode at the exterior, quarter points of the center span, the data predict a mean frequency of 14.484-Hz with a standard deviation of 0.122-Hz. While the two center span quarter-points feature a little out of phase vibration of the inner edge at this frequency, there is little other motion excited by this mode with the exception of some minor vibration on the end spans that tends to be in-phase with the adjacent, center

quarterspan, as seen in Figure 16. This motion is not very evident in the frequency domain signals except when the mode is excited by a direct impulse at the center span quarter-point, and then the amplitude varies significantly, suggesting that the data amplitudes may be receiving interference from the nearby eleventh mode. Examining the data from the quarter-point impulses alone shows that the interior edge of the center span has a distinct, albeit small, motion opposite that of the exterior edge, suggesting that the mode combines a little twisting with bending. The averaged data failed to reflect this characteristic, however.

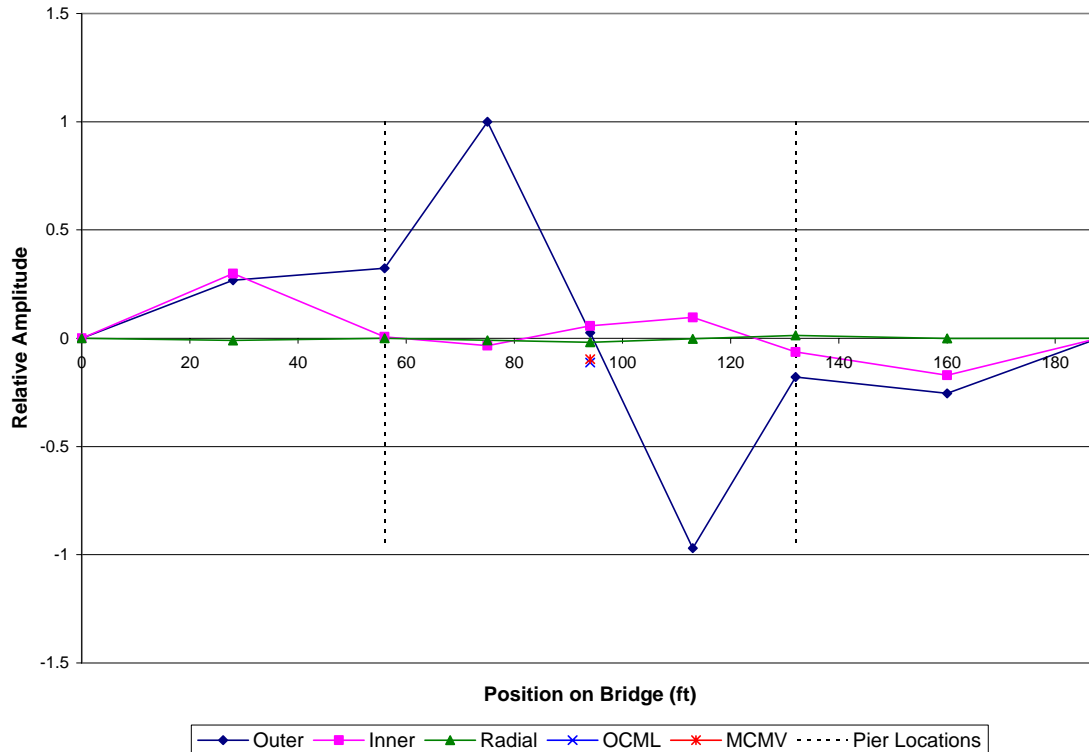


**Figure 16. Tenth Mode: 14.484 Hz ± 0.122 Hz**

One other notable characteristic of this mode is that, upon examining the frequency domains from each of the excited locations, this mode appears to have a great deal of damping in it. Especially in comparison to the first, third and even ninth modes, the base of the peak at this frequency is much wider, in one instance seemingly effecting a range of about four-Hertz. Having three strong modes within that four Hz range might have exacerbated this apparent spread, but they seem to have minimal impact on a strictly visual analysis. This might be why the mode does not seem to be noticeable at most of the locations other than the exterior, center span quarter-points. Separating the data into two groups by the trip during which they were collected, there is a notable difference in measured data. While there is much more overlap between the data obtained during the two trips than there was for the ninth mode, as is indicated by their standard deviations, data collected during the third and fourth trips predicted mean natural frequencies of 14.603-Hz and 14.434-Hz, with standard deviations of 0.121-Hz and 0.082-Hz, respectively.

## Eleventh and Twelfth Modes

The eleventh and twelfth modes present the second case where two modes were sufficiently close together that significant interference occurs between the frequency domain data. When the data were accumulated and averaged into a single mode shape, the right end of the bridge showed the strong amplitude that the frequency domain representation indicated it would have, but the left end seemed to have none even though its frequency domain showed that it was nearly as strong as the right. Looking at the individual data points, the problem became clear. The eleventh and twelfth modes both have strong motion of the two end spans, but one is symmetrical, while the other is anti-symmetrical. When the left side was being averaged, the data that belonged to what turned out to be the eleventh mode was of an out of phase, negative amplitude and when combined with the in phase, positive amplitude data that belonged to the twelfth mode, the motions canceled each other out. This was obviously not the case on the bridge itself. Thus, it is possible to separate the two modes to a certain extent. One limitation in the ability to identify these modes is that both modes appear to have significant end span hogging, which could not be specifically verified because no accelerometers were placed midway across the end spans. The contrasting nature of these two mode shapes is also seen from the FE models, which are discussed later.

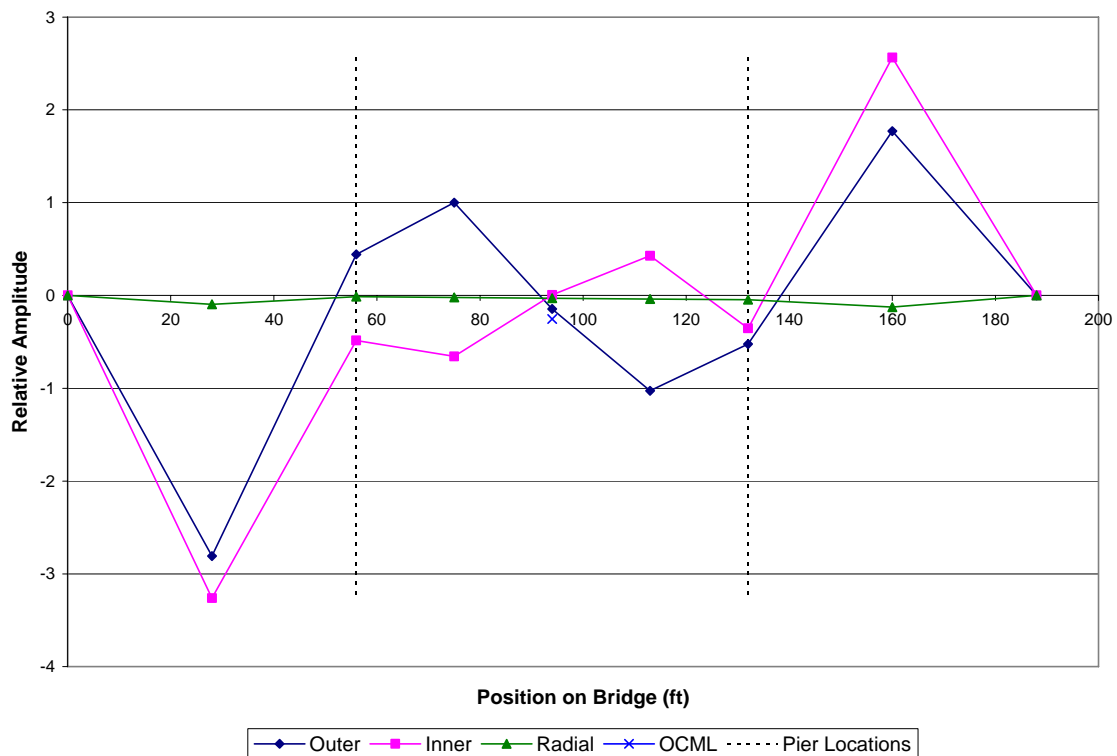


**Figure 17. Eleventh Mode: 15.147 Hz  $\pm$  0.091 Hz**

Using the aforementioned distinction between the modes, it was possible to separate the data into two groups and average them separately. It becomes readily apparent that though both modes have dominant end span motion, the motion of the two end spans is out of phase in the eleventh mode, but in phase in the twelfth mode. Further examining the transformed data, it became apparent that there are actually two peaks very close together in most locations. For two

modes that are so similar, it may be difficult to isolate them any further even with a single shaker, since it may be hard to find a point on one mode that is a node that undergoes significant displacement in the other mode. It may be possible to isolate the two modes with dual shakers driven in phase to excite the twelfth mode and out of phase to excite the eleventh mode. Thus it is difficult to be too confident about the precision of the two frequencies, or the amplitudes of the mode shapes. The separated modes are shown in Figure 17 and 18, and clearly show the difference in phases between the endspans. Mode 12, shown in Figure 18 also shows that the mid-point of the center span is out of phase with the inner and outer edges, suggesting that hogging motion of the deck is occurring in that mode. The displacements on the center span are relatively small, so little confidence can be had in those displacement amplitudes.

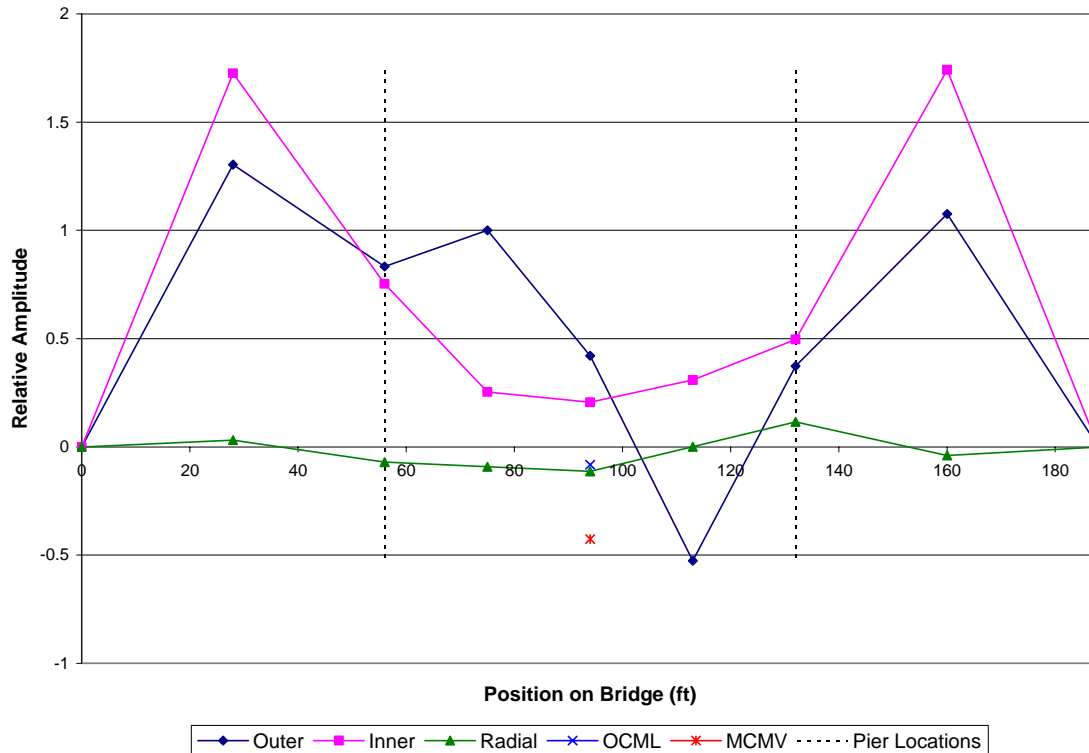


**Figure 18. Estimated Twelfth Mode: 15.363-Hz**

The eleventh mode appears to be the slightly lower of the two frequencies, averaging a natural frequency of 15.147-Hz with a standard deviation of 0.091-Hz, while the twelfth mode was determined to have a natural frequency of 15.363-Hz with a standard deviation of 0.053-Hz. The precise values of these frequencies are somewhat dubious, since the two modes are closely spaced, and there is significant overlapping of measured frequencies, in one case seeing out of phase end span motion, the defining characteristic of the eleventh mode, as high as 15.381-Hz.

The two center spans of each mode both contain a reversed curvature bending motion on the outer edge, but while the eleventh mode appears to contain an apparent torsional motion on the inside curve, the twelfth mode has minimal motion on the center span. The reversed curvature seen in the twelfth mode center span is not consistent with the hypothesized symmetry of that mode, a further indication that mode twelve is not closely identified.

## Higher Modes

Along with the previous twelve modes that were analyzed in depth, numerous higher natural frequencies were measured on the bridge. By sampling data at 100 samples per second the transformed signals should be able to fairly confidently record frequencies as high as 50-Hz, according to the accepted limits of the FFT. However, it is somewhat difficult to be precise about the associated mode shapes, because of the relatively small number of accelerometers locations, and the increasing complexity of the mode shapes. Fortunately only a few frequencies appeared at all above the first twelve, and so while they will be briefly mentioned, and shown if possible, they were all generally relatively weak, especially in response to vehicular excitations.

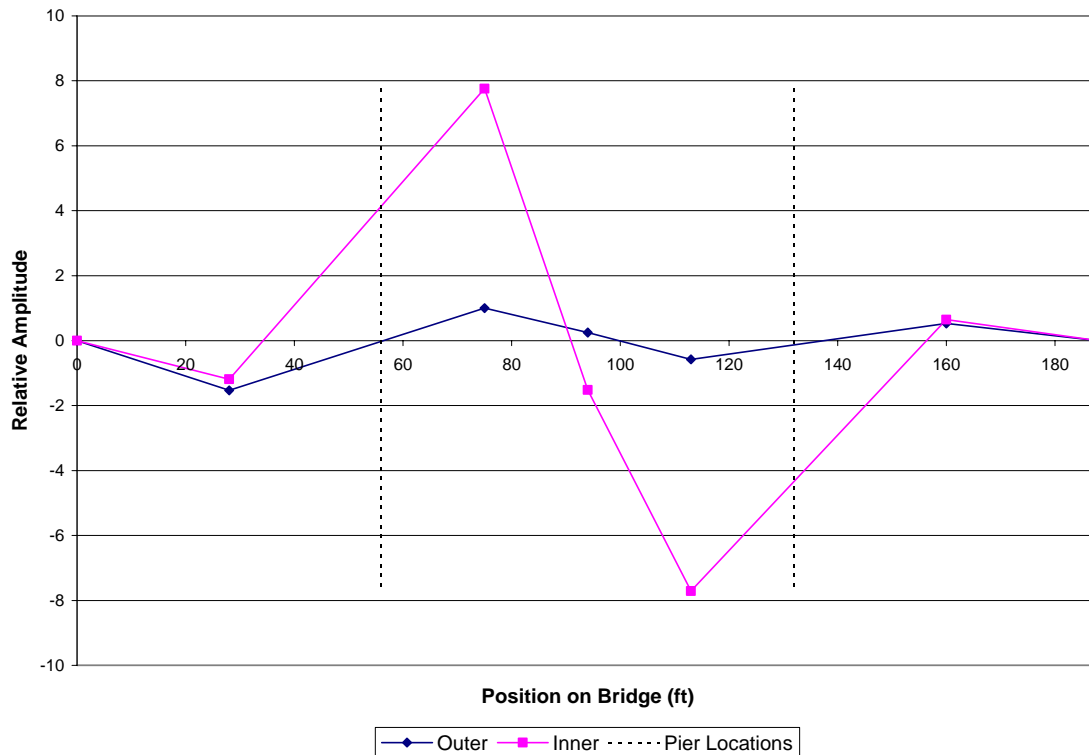


**Figure 19. Thirteenth Mode: 17.168 Hz  $\pm$  0.175 Hz**

The thirteenth mode was only excited by van runs, and only five FFT plots were available to average, none of which provided any data at the pier locations or in the radial direction, but it still managed to form a reasonably consistent shape as found in Figure 29. The data actually gave an average natural frequency of 17.168-Hz but had a notably high outlier as shown in the standard deviation of 0.1855-Hz.

The finite element models actually produce three or four extra modes before the next significant data peak in the field data generates what will be referred to as the fourteenth mode at about 20.7-Hz. Fairly consistent data were available at this frequency, resulting in a reasonable mode shape, as shown in Figure 20, but the mode itself never produced a very strong peak to warrant the amount of consideration that the lower frequencies demanded. However, it is significant to note that this was a mode that was noticeably excited during the van runs.

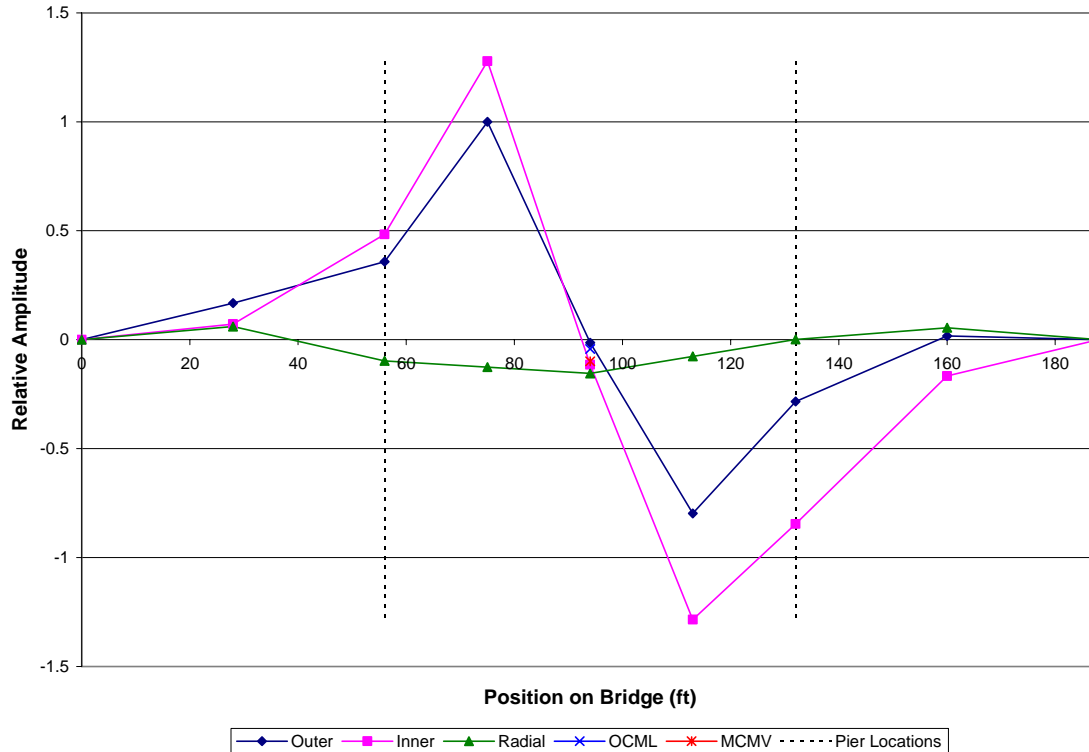


**Figure 20. Fourteenth Mode: 20.672 Hz ± 0.089 Hz**

With a mean natural frequency of 20.672-Hz and a standard deviation of 0.089-Hz, the fourteenth mode is anti-symmetrical about the center of the bridge and shows reversed curvature bending of both the inner and outer edges that is accompanied by significant relative motion in the piers.

The last frequency that the shaker appeared able to excite into was found at 23.995-Hz with a standard deviation of 0.108-Hz,. As Figure 21 shows, the mode apparently includes a significant amount of motion at the exterior mid-point of the center span, while the interior mid-point of the center span seems to level off with the quarter-points. Also curious is that while the mid-point of right end-span is symmetrical about the centerline, the midpoint of the left end-span is anti-symmetrical about the centerline.

Additional higher frequency peaks were consistently found at around 25.2-Hz, 28-Hz, and 36-Hz, though the peaks generally appeared more as rolling mounds that covered a span of as much as 6-Hz at times and never presented any consistent or recognizable shapes to summarize.

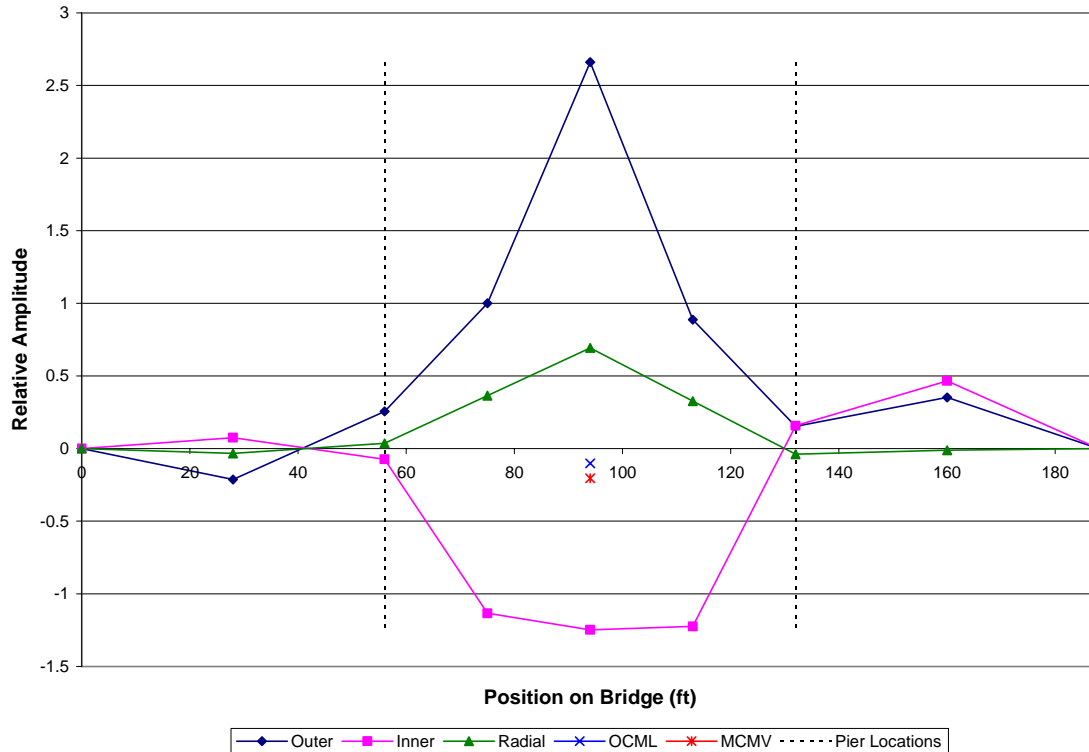


**Figure 21. Fifteenth Mode: 23.995-Hz  $\pm$  0.108 Hz**

## DISCUSSION

The Wolf Creek Bridge is a nearly symmetrical structure. Deviations from complete symmetry are minor, and include a small elevation difference between the two ends, and an orientation of diaphragm channel legs that does not attempt to maintain symmetry. Therefore, most of the lower modes were expected to be nearly symmetrical, or nearly anti-symmetrical, unless boundary conditions exist that destroy symmetry. Such boundary conditions could include pinned bearings that have frozen against rotation, or roller bearings that have developed a large resistance to translation. Because of horizontal curvature of the bridge, the usual vertical bending modes and torsional modes displayed significant coupling. However, it is possible to distinguish between three types of vertical bending/twisting behavior: outer edge bending, with some twisting and relatively little inner edge motion; inner edge bending, with some twisting and relatively little outer edge motion, and torsion, with almost equal magnitudes of motion of the inner and outer edges. In addition to these modes, several modes display “hogging” or transverse bending characteristics.

Originally, two finite element models were developed by Lydzinski (2006). The first model assumed rigid piers, while the second model explicitly included flexible piers. In the sequel, the first model will be referred to as Lydzinski’s rigid pier model (LRPM), while the second model will be called Lydzinski’s original flexible pier model (LOM). LRPM results did not agree particularly well with the measured data, so it is only considered briefly in the discussion.

## An Unexpected Boundary Constraint

According to LOM, the bridge's first mode should be a first-order rotational vibration dominated by an almost rigid body rotation of the bridge superstructure about the center of curvature on a vertical axis of rotation, accompanied by minor vertical bending. at 2.281-Hz. The second mode shape should be bending of the entire deck in the radial direction with significant rotation of the pier caps about the tangential axis and tangential translation of bridge ends at a frequency of 3.62 Hz. The predicted first mode reflects the piers' flexibilities in a tangential direction, while the second mode incorporates the piers' rotational flexibilities. Both modes also reflect the assumed roller-like boundary conditions at the two abutments. During the preliminary trip to the bridge, resonant frequencies were identified at around 2.3-Hz and around 3.2-Hz, so there was no perceived problem with the modeling, although the second frequency was somewhat lower than predicted, suggesting that the piers' true rotational stiffnesses might be somewhat lower than modeled.

When these natural frequencies were not found during the second and third trips, and several other notable discrepancies between the field data and the FE analysis were observed, the computed mode shapes were examined more closely and it was realized that none of the accelerometers had been oriented to pick up the tangential motion characterizing the first mode. It was not clear at that time why the radially oriented accelerometers had not picked up the second mode. Therefore, during the final trip to the bridge an accelerometer was set up in the longitudinal (tangential) direction and an impulse hammer was used in an attempt to excite the bridge in these modes. It was decided that only one accelerometer was needed to verify the existence of the first mode because the predicted dominant motion is primarily a simple first order rotational motion about the center of curvature of the bridge, and a single accelerometer placed tangentially is capable of measuring this motion.

It was decided to impact the railing at the end of the bridge, with the thought that any impact location should be essentially equivalent, since the objective was to create a moment impulse about the center of curvature. Several impulses were applied to the bridge in this manner, but the resulting acceleration signals showed negligible tangential motion. This was somewhat surprising, given LOM's prediction that the 2.3 Hz mode is the fundamental vibration mode. Consequently, the end boundary conditions of the bridge were examined more closely to determine whether additional constraints against tangential motion might exist.

During testing, it was noticed that steel highway safety railings are connected to the bridge terminal walls at each end. Since these guardrails are designed to allow for thermal expansion, they were originally not given much thought. After the impulse hammer failed to produce any tangential motion, the significance of the safety railing was reevaluated. Upon closer inspection, the actual connections of the metal guardrail to the bridge appeared more rigid than had previously been assumed. The slotted-bolt connections necessary for the thermal expansion were only found on two of the four attachments, diagonally opposite to each other. That would allow for the inside and outside to expand, but at opposite ends of the bridge rather than all together, possibly resulting in an added shearing to occur parallel to the roadway, but most certainly altering any rotational modes of the bridge. The slotted-bolt connections were relatively tight, leading to the hypothesis that, while slippage would be possible under a

sufficiently large constant force such as that caused by thermal expansion or contraction, a considerable amount of friction probably exists that would tend to prevent any tangential motion under small impulse loadings. This observation suggests that slippage could conceivably occur under large vehicular loadings, but that the modal identification procedure might be incapable of picking this up.

### Finite Element Model Modifications

To test the theory that the guardrails are restraining motion, the flexible pier ANSYS model was modified. Not having the railing's properties readily available, and not wanting to significantly increase the size of the model, the most straightforward approximation was to fix the terminal walls against motion in the tangential direction. Two approximations were developed. In the first approximation, referred to as the "fixed railing" model, two nodes at different vertical locations were constrained against tangential motion at the ends of each terminal wall. In the second approximation, called the "pinned railing" model, only a single node was constrained at the end of each terminal wall. Although these approximate models oversimplify the actual condition imposed by the end railings, and may overestimate the attachments' stiffnesses, the models were considered to be reasonable estimates that provide upper bounds to the added stiffness. It was also expected that the support with no railing restraint provides a lower bound estimate.

One difficulty with the idea of end railing induced restraint is that the low frequencies (2.3 Hz and 3.2 Hz) had been found during the preliminary trip to the bridge. Examining photographs taken during the first trip resolves this issue and tends to further validate the hypothesis that the end railings are preventing the low frequency modes. As shown in Figures 22 and 23, the guardrails had not been attached at the time of the first trip.

The first fifteen natural frequencies obtained from the field analysis are compared with the first 20 frequencies predicted by the four FE models in Table 3, with the comparison based upon both frequencies and mode shapes. In addition, the first two modes of LOM without end restraint are included in the tabulation. Both of the new modeling approximations appeared to improve upon Lydzinski's original flexible pier model. Not only is the first mode eliminated, but the second mode that was originally around 3.6-Hz disappears and a new mode appears at around 5.7-Hz that reasonably matches the motion of the second mode from the field data.



Figure 22. Guardrail Attachment Absent



Figure 23. Guardrail Attachment Present

**Table 3. Measured and Predicted Modal Frequencies Comparison**

Found Mode No.	FE w Rigid supports (Hz)	FE w/o Railing Connection (Hz)	FE w/ Fixed Railing (Hz)	FE w Pinned Railing (Hz)	Measured Frequencies (Hz)
	-	2.281	-	-	-
	-	3.619	-	-	-
1	5.871	4.654	4.594	4.561	4.565
2	-	-	5.683	5.652	5.215
3	7.407	6.271	6.523	6.434	6.500
4	7.787	7.338	7.627	7.334	7.396
5	8.905	8.230	8.715	8.552	8.730
6	10.359	8.817	8.995	8.824	8.915
7	10.603	9.642	10.644	10.509	10.188
8	14.449	10.797	11.390	11.266	10.505
9	14.221	13.640	13.649	13.644	12.186
10	15.294	13.478	13.444	13.416	14.484
11	16.294	15.251	14.755	14.706	15.147
12	16.320	15.790	16.002	15.891	15.363
13	17.109	16.033	15.961	15.938	17.168
	18.964	17.979	18.135	17.053	-
	-	19.665	18.610	18.077	-
	-	-	20.227	19.747	-
	21.189	20.312	20.654	20.504	-
14	22.893	21.251	21.420	21.333	20.672
	-	22.830	22.976	22.873	-
	24.057	-	24.621	24.286	-
15	24.350	23.756	-	-	23.995

**Field Data - Finite Element Model Mode Comparisons**

Comparison of measured and predicted modes required both qualitative and quantitative assessment approaches. All models predicted a number of modes within the range of the measured frequencies, so an initial comparison attempted to match overall mode shapes from the particular models with the measured shapes. Once the mode shapes were visually matched as well as possible, two quantitative measures were used, although not exhaustively. Two measures of the prediction quality are the natural frequency and the relevant displacement ratios. The frequency comparison could be used in every case, while a quantitative comparison of mode shape relative amplitudes was used on a case by case basis. In all cases, the initial objective was to assist in mode shape identification, and the secondary objective was to verify the appropriateness of the particular FE model. In the discussion below, primary reference is made to the order of the measured mode, since the different FE models predicted the modes in somewhat different orders in several cases. The mode shapes obtained from the pinned-rail model are shown in the Appendix. The mode shapes from the rigid pier model, LOM and the fixed-rail model can be found in Turnage (2007).

**First Mode**

Both modes 2 and 3 of LOM bear some resemblance to this mode. LOM mode 2 predicts significant inner edge bending opposite that of the outer edge, while mode 3 predicts some inner

edge bending in phase with the outer edge. By comparison, the measured data indicate that very little vertical motion of the inner edge is occurring. Thus, neither mode of LOM predicts the measured shape particularly well. The measured mode shapes showed side span displacement amplitude/center span displacement amplitude ratio of 30% on the dominant outer edge. By comparison, the third mode of LOM, chosen because of its closer agreement with the measured frequency, predicted a ratio of 50%. LOM mode 2 predicts a frequency of 3.619 Hz, 20.8% below the measured frequency, while mode 3 predicts 4.654 Hz, 1.86% above the measured frequency.

By contrast, this modal frequency was predicted reasonably well by both constrained FE models, although the pinned railing model appeared to provide the closer prediction. The fixed railing model predicted 4.594 Hz, 0.55% above the measured frequency, and the pinned railing model predicted 4.561 Hz, 0.09% below the measured frequency. The fixed rail model predicted a displacement ratio of 20%, and the pinned railing model predicted a ratio of 24%. This suggests that the fixed rail model significantly over-constrains the ends, while the pinned railing model only slightly over-constrains the ends, while providing a relatively realistic model.

## **Second Mode**

The second mode is strongly influenced by the guardrail attachment end conditions, and by the pier flexibility, as evidenced by the significant pier rotation shown by the relative displacements between inner and outer pier transducers shown in Figure 9. LOM does not reproduce this mode, which is dominated by inside edge bending, very well. LOM mode 2 at 3.619-Hz slightly resembles this mode, but with the vibrations on the outside edge of the bridge exceeding that on the inside edge of the bridge, and with much larger radial bending displacement of the deck, accompanied by unrestrained rotation of the ends of the bridge about a vertical axis. The motion features significant bending of the piers about a tangential axis and substantial radial motion of the deck, and that motion is probably what was detected during the first trip to the bridge, although at around 3.2-Hz, slightly lower than predicted by LOM.

During the initial data analysis, this mode was thought to resemble the shape of the mode that LOM showed at 6.271-Hz, which is a predominately center span, inside bending vibration. However if that were the case, then the discrepancy between the measured (5.215 Hz) and computed (6.271 Hz) frequencies is unacceptably large. An additional problem then arises in that the field data provide a second 6.6-Hz frequency. These problems substantially disappear when considering the modified FE models with the ends restrained.

The revised models, though providing a significant improvement in predicting this mode, are not perfect. The fixed rail model predicted the natural frequency to be 5.683-Hz, (9% high), while the pinned rail model predicted a frequency of 5.652 Hz, (8.4% high). Thus, both of these models are slightly too stiff. Both of the modified FE models indicate that the outer edges of the end spans undergo larger displacements than the outer edge of the center span, which does not agree with the measured data. There are a couple of possible explanations of the discrepancy. The most likely explanation is that the pier rotational stiffness is somewhat overestimated by the FE model. A second possibility is that both of the modified FE models apply too rigid a

constraint at the ends, although the excellent agreement of the pinned end model's first mode, for which the measured pier rotation is relatively small, makes that less likely.

### **Third Mode**

The finite element models predicted this mode reasonably accurately, with the possible exception of the relative amplitudes. LRPM picked up this mode at 7.407-Hz, but the mode shapes had very little motion in the exterior spans and portrayed the center span as having almost exactly the same amplitudes on the outside and inside edges, albeit in opposite directions, suggesting that the absence of pier flexibility tends to reduce the amount of coupling between spans significantly. LOM did a somewhat better job of capturing the mode shape, but underestimated the movement along the inside edge of the center span and the outside edge of the exterior spans. LOM predicted a frequency of 6.271-Hz, about 3.5% lower than was found on the actual bridge. The pinned rail FE model was slightly too flexible, at 6.434 Hz, (-1.01% error). The fixed rail FE model closely predicted the natural frequency as 6.523-Hz (0.53% error), which is less than a single step in the frequency domain and well within a standard deviation of the averaged field data.

All of the flexible pier FE models predicted somewhat larger motion along the outside edge of the center span than was measured. The measured ratio of outside edge to inside edge vertical acceleration was 0.30. By contrast, the LOM predicted a ratio of 0.556, the fixed rail model predicted 0.698, and the pinned rail model predicted a ratio of 0.663. This suggests that the FE models may predict somewhat stronger coupling between inside and outside edges of the bridge than actually exists.

A further anomaly that this mode presents was that the shaker-induced excitations produced a somewhat lower frequency estimate than the impulse and vehicular excitations. While the first trip produced large shaker-induced motions at around 6.8-Hz, the third trip produced resonant motion initially around 6.6-Hz, but later only around 6.36-Hz. By contrast, impulse and vehicular excitations, including the majority of those from the third trip, tended to be closer to the 6.5-Hz range. The discrepancies of the first trip can be explained by the absence of the guardrails and the likelihood that a different mode was being measured. There was not any obvious reason why the measured data on the third trip should differ significantly from the data obtained during the fourth trip. However, a number of researchers have observed that dynamic response data may be temperature dependent, and this possibility cannot be ruled out.

### **Fourth Mode**

The fourth mode is an anti-symmetric mode, dominated by bending of the outside edge of the end spans. Therefore, it would appear that this mode would be particularly sensitive to the degree of end restraint imposed by the guardrails. All of the models, including the rigid pier model, reproduced the mode shapes relatively well. LRPM predicted a natural frequency of 7.787 Hz, over-estimating the measured 7.396 Hz natural frequency by 5.3% and suggesting once again that the pier flexibility cannot be ignored. Mode 4 of the fixed rail model also over-estimated the frequency, predicting 7.627 Hz, which is 3.1% high. By comparison, mode 5 of LOM predicted 7.338 Hz, about 0.79% low, and the pinned rail model predicted 7.334 Hz, about

0.84% low. This mode does not display any strong tendencies for tangential motion of the ends, so the pinned rails would not be expected to have a strong effect upon the natural frequency, and this was indeed the case. This mode provides further verification that the fixed rail assumption may produce a model that is too stiff, while the pinned rail assumption may be a reasonable approximation. In particular, the fixed rail model provides significant constraint against end-span rotation at the abutments, while it is unlikely that the guardrails would be able to do this.

### **Fifth and Sixth Modes**

The modified FE analyses appear to predict these two modes reasonably well, and they certainly help in separating them. All of the FE models show two distinct modes near these frequencies. All of the FE models have a mode that closely matches the motion of the outer edge of the bridge shown in Figure 12 and a second mode at a slightly higher frequency that again closely matches the motion on the inside edge of the bridge. However, none of the FE models combine the two motions, and neither mode seems to have an effect on the opposite edge of the bridge in either of the pier models. The one case where the non-dominant edge shows significant motion is on LRPM, which while it separates the two modes far more than the other two models, does present a case where the fifth mode shows twisting motion about the longitudinal centerline of the bridge. LOM estimates the two modes (modes 6 and 7 in that model) at 8.23 Hz (5.7% low) and 8.817 Hz (1.1% low), respectively. The fixed end rail FE analysis estimates the two modes at natural frequencies of 8.715-Hz (0.17% low) and 8.995-Hz (1.37% high) for the fifth and sixth modes. The pinned end rail model estimates frequencies of 8.552 Hz (2.0% low) and 8.824 Hz (1.0% low). All of the FE models predict that the fifth mode is symmetrical, with outer edge motion of the end spans dominant, while the sixth mode is anti-symmetrical, with inner edge motion of the end spans dominant. In this case, the fixed rail model appears to provide the best frequency estimate for the fifth mode, while LOM provides the least accurate model. This would suggest that the fixity against rotation might be somewhat greater than was previously thought. It is believed that this is not the case, and that other sources of the model flexibility in the fifth mode need to be considered. One possibility is that the FE models admit some local bending in the outer edge of the pier caps that lower the natural frequency of the mode that is dominated by outer edge symmetrical motion. This possibility is not inconsistent with the previous hypothesis introduced in connection with mode 2 that the overall rotational stiffness of the pier may be overestimated, since the former hypothesis rests on local pier cap stiffness, while the latter hypothesis rests on overall rotational stiffness of the pier.

The significant overlap of the two signals in the frequency domain, together with the fact that one dominates on the outer edge, while the other dominates on the inner edge made it initially difficult to separate the two signals to obtain clean mode shapes. Somewhat more realistic mode shapes are obtained if the amplitudes obtained from the rudimentary analysis are separated into symmetric and anti-symmetric functions. This leads to the two graphs plotted in Figures 24 and 25, which agree quite well with the expected shapes of the two modes. One must be careful in drawing too strong a conclusion from the appearance of these graphs, however, since it is much easier to construct true symmetry in a mathematical model than to demonstrate that it exists in an actual structure, no matter how symmetrical the structure may *appear* to be.

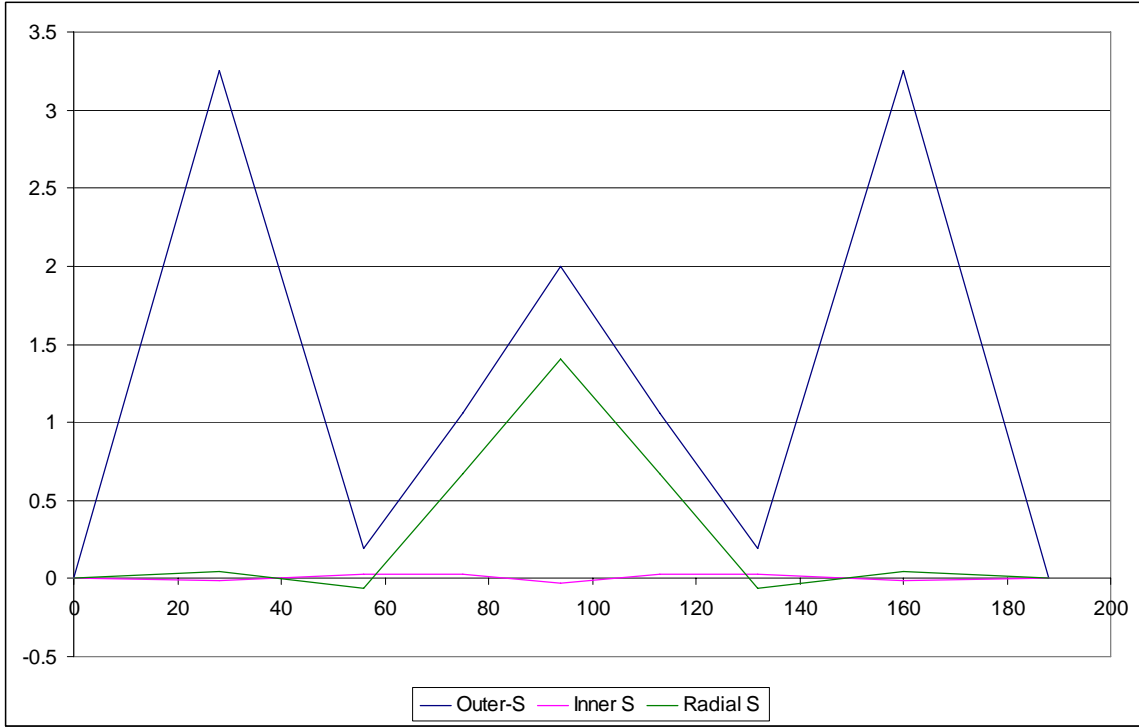


**Figure 24. Symmetric Part of the Measured Mode 5/6 Shapes**

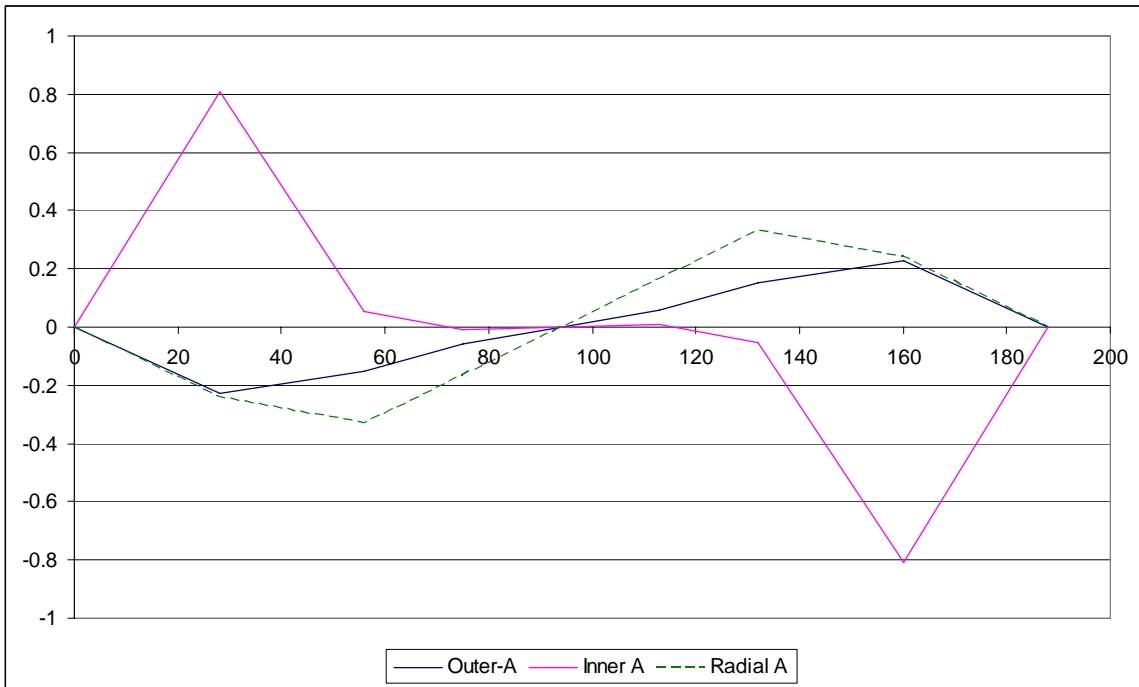


**Figure 25. Anti-symmetric Part of the Measured Mode 5/6 Shapes**

## **Seventh Mode**

Mode seven is a symmetrical mode, dominated by bending of the inside girders on the end spans. The measured mode does not completely achieve symmetry, but does display nearly symmetrical motion. With the exception of these amplitude irregularities, this mode falls into a fairly consistent pattern with several previous modes in their comparisons to the finite element analyses. In this case LOM predicts a natural frequency of 9.642 Hz (5.4% low); the pinned-railing model predicts 10.509 Hz ( 3.2% high); and the fixed-railing predicts a frequency of 10.644 Hz (4.48% high). This would further suggest that the ends are substantially, but not completely restrained against translation by the guardrails, but that rotational restraint, if present, is limited. Direct comparison of the measured mode shapes with the predicted mode shapes is of somewhat limited utility here, because of the relatively limited precision of the measured mode shapes.

## **Eighth Mode**

The measured eighth mode is an anti-symmetrical mode dominated by second mode torsion of the center span. The mode shape predicted from the field data agrees reasonably well with the flexible pier finite element analyses. The measured mode shape displays some deviations from anti-symmetry, which is not surprising, since the actual structure may not be quite symmetrical. Even if the true mode shape is anti-symmetrical, the data are unlikely to reproduce the increasingly complex mode shapes of the higher modes precisely. All of the FE models slightly over-estimate the natural frequency. LOM does the best job, predicting a frequency of 10.797 Hz (2.78% high). The pinned rail model is slightly stiffer, predicting a frequency of 11.266 Hz (7.2% high). The fixed rail FE model predicts a natural frequency of 11.390 Hz (8.4% high). The mode shapes predicted by the FE models indicate the presence of significant pier cap rotation in this mode. Taken together with the observation from the second mode this reinforces the hypothesis that the FE models may overestimate the piers' rotational stiffnesses.

## **Ninth Mode**

The ninth mode reflected the first time that the FE models predicted modes in a different order than the field data. Matching this measured mode up with the FE models showing transverse motion was still straightforward, provided the correct mode was examined. However this mode corresponds to the tenth mode of the pinned-rail and fixed-rail models, and to the eleventh mode of LOM. None of the FE models predicted the natural frequency very closely. LOM, the pinned rail model and the fixed rail model predicted very similar frequencies for this mode at 13.640-Hz (11.93% high), 13.644 Hz (12.0% high) and 13.649-Hz (12.0% high), respectively, indicating that the guardrail boundary condition has little effect on this mode. This is not surprising, since the mode is dominated by hogging of the center span.

The FE models representation of mode shapes do not agree particularly well with the measured mode shapes. The FE models predict very little motion at the end spans, while the field data show distinct peaks on the FFT graphs at all four end span locations. Likewise, the FE models predict somewhat larger relative amplitudes at the middle of center span relative to the

edges than was measured in the field. Several factors could contribute to these errors. Bending of the railings contributes significantly to the mode shapes, and it is possible that the FE models have overestimated the effective contribution of the railing stiffness to the model. Also, it is possible that the FE models have overestimated transverse coupling somewhat, either by overestimating the stiffness of the slabs, or by overestimating the stiffness of the diaphragm connections. Finally, the stiffness of the superstructure to pier cap connection may be too high. It is also possible that some combination of these factors may be present.

### **Tenth Mode**

The tenth mode is dominated by second mode anti-symmetric bending of the outer edge girder. A small amount of end span bending also occurs, but this mode is not expected to be particularly sensitive to the end boundary conditions. All three finite element models produce similar mode shapes, which resemble the predicted mode shape but tend to underestimate the natural frequency. The LOM, pinned railing and fixed railing models provide frequency of 13.478-Hz. (6.94% low), 13.416 Hz (7.37% low) and 13.444 Hz (7.18% low), respectively.

A curious aspect of this mode is that adding the guardrail boundary condition reduced the predicted frequency of this mode rather than stiffening the mode as has happened to every prior mode. The mode shapes predicted by all three models seem to be fairly reasonable, even showing the subtle anti-symmetry between the edges of the center span. In contrast to the three flexible pier models, which reverse the order of the ninth and tenth modes, LRPM has the two modes in the correct order, although the frequencies are significantly over-estimated.

### **Eleventh Mode**

The finite element analyses were helpful in determining this mode experimentally. However they do not capture the mode shape particularly well. The eleventh mode is anti-symmetrical, and dominated by end span motion. The frequencies predicted by LOM, pinned-rail, and fixed rail models, respectively, were 15.251 Hz (0.69% high), 14.706 Hz (2.9% low) and 14.755 Hz (2.6% low). The anti-symmetric nature of the mode is reflected in all three FE models. However, all models predicted that the largest displacements occurred on the outer edge of the bridge, while the measured mode shapes predicted larger displacements on the inner edge. The models also indicate the presence of some hogging motion of the end spans. This could not be verified using the measured data in the absence of data from additional accelerometer locations.

Two modes generated by the finite element analyses (modes 11 and 14 of the pinned-rail and fixed rail models, and modes 12 and 14 of LOM) had very similar motion to the eleventh mode, both showing out of phase, transverse bending motion on the end spans and second-order motion on the center span. The most significant difference in the generated modes was that the interior, center span, quarter point vibration of the lower frequency was in phase with its adjacent, interior end span vibration as was the case for the measured mode, while the higher modes had them out of phase with each other. It appears that the lower mode numbers match the frequency and shape of the measured mode more closely than the higher mode numbers. Thus, the lower predicted mode numbers were assumed to correspond to the measured eleventh mode.

The measured motion of the exterior center span in the eleventh mode suggests that the proximity and previously mentioned damping of the tenth mode may have influenced the predicted shape of this mode. If the tenth mode's anti-symmetrical motion is overlapping with this mode, it would also help explain why the predicted relative amplitude of the center span motion is so much smaller than the end spans motion.

## **Twelfth Mode**

After separating the twelfth measured mode from the eleventh mode, it appears that the data tend toward a symmetrical mode. The dominant inner edge data display significant symmetry, as do the outer edge data on the end spans. However the center span data on the outer edge deviate significantly from symmetry. The proximity of this mode to the anti-symmetric eleventh mode has probably made accurate prediction of the twelfth mode shape difficult.

In this mode, there is some change in order of the FE models' modes. The thirteenth mode predicted by LOM is essentially symmetrical, and dominated by end span motion. By contrast, both the pinned-rail mode 12 and fixed rail mode 13 predict a small deviation from symmetry, with generally similar mode shapes. The dominant motion predicted by these models is nearly symmetrical end span bending plus substantial hogging. The FE models predict that inner edge motion should be somewhat larger than outer edge bending.

The twelfth mode frequency was easier to match up with the FE models, although it was not as accurately captured by the field data. LOM predicted a modal frequency of 15.790-Hz, (2.8% high), the pinned rail model predicted 15.891 Hz (3.4% high) and the fixed rail model predicted 16.005-Hz, (4.2% high). With that exception, and again assuming that the measured center span motion is influenced by overlap with measured mode eleven, and possibly ten as well, the models are in fairly reasonable agreement with the data.

## **Higher Modes**

### *Thirteenth Mode*

The thirteenth mode measurements did not display significant overlap with adjacent modes, so extracting this mode was fairly straightforward. The anti-symmetric motion of the mode is dominated by reversed curvature bending of the center span's inner edge. The measured mode shape appears to correlate well with mode 14 of LOM, mode 13 of the pinned rail model and mode 12 of the fixed rail model. In this case as well, all of the FE models underestimate the natural frequency, with LOM performing best. LOM predicts a frequency of 16.033 Hz, (6.6% low), the pinned rail model predicts 15.938 Hz (7.2% low) and the fixed rail model predicts 15.961 Hz (7.0% low).

### *Fourteenth Mode*

The fourteenth mode also shows anti-symmetric, reverse curvature bending of the main span, but for this mode, both inner and outer edges appear to undergo comparable motion. The measured edge motion of this mode appears to match mode 18 of the three FE models most

closely. Complete verification of this measured mode would require additional transducers located at the centerline of the quarter spans, since the FE models predict significant second mode hogging of the deck. All three FE models over-estimated the natural frequencies, which is consistent with earlier hogging modes, reinforcing the hypothesis that the models have overestimated the transverse bending stiffness of the superstructure. The LOM, pinned rail and fixed rail models predict 21.251 Hz (2.8% high), 21.333 Hz (3.2% high) and 21.42 Hz (3.6% high), respectively.

### *Fifteenth Mode*

This motion does not match any of the computer generated mode shapes. It appears to be dominated by torsion of the main span, and almost no motion of the side spans. The high measured frequency, in comparison with the similarly shaped mode 3 suggests that some additional local deformation may be occurring that has not been measured by the limited number of transducers.

## **CONCLUSIONS**

This project had fairly specific objectives in its application to a single bridge, however there are some general conclusions that can be applied to future vibration tests and/or bridge modeling.

- A straightforward automated process can identify the natural frequencies of a reasonably damped, noisy bridge very well.
- Impulse excitations are an excellent means of exciting a curved girder bridge in order to gather vibration data. For complete sets of data, these impulses should be made at the mid-span at all spans on both the inside and outside of the bridge as well as the quarter-spans of any spans that are expected to have second-order bending modes within the frequency range that is being analyzed.
- The flexibility of the piers of the Wolf Creek Bridge contributed significantly to the dynamic response of the bridge, as hypothesized by Lydzinski (2006). The accuracy of the simplified pier model may need to be improved upon, as certain of the modes suggested that the rotational stiffness of the pier model may be too high, while the bending stiffness of the pier cap may be too low.
- The standard metal guardrails that are attached to the ends of the bridge have a high level of stiffness in the direction parallel to their length, incorporating themselves into the structural system and altering the dynamic response of the bridge. Translational constraint is more significant than rotational constraint.
- Measured transverse (hogging) modes appear to be less stiff than modeled by the FE models, suggesting that the diaphragm model connections and/or the slab are too stiff in the FE models.

## RECOMMENDATIONS

Several lessons were learned during this study that can lead to improved results in future field tests. Therefore, the following recommendations regarding future studies are provided for bridge researchers.

### Field Testing

1. *Bridge researchers should begin with a series of preliminary impulse studies that can provide a list of likely frequencies for future testing.* The impulses need to be applied at a variety of locations on all spans of a multi-span structure with the intent of exciting as many modes as possible.
2. *Bridge researchers should consider the use of larger impulse sources such as falling weight deflectometers should be explored.*
3. *Bridge researchers should consider shaker excitation for follow up excitation once natural frequencies have been approximately located.* A properly spaced shaker can provide reasonably precise frequency identification once the general location of the frequency is known.
4. *Bridge researchers should recognize and exploit symmetry whenever it is present, specifically looking for symmetric and anti-symmetric modes.* Excitations specifically designed to excite such modes should be considered.
5. *Bridge researchers should consider additional transducers to provide a sufficiently dense array for full modal identification.*
6. *Bridge researchers should consider more sophisticated time and frequency domain methods that can back out damping estimates.* These methods have been developed, and should be critically evaluated for inclusion in future projects.

### Finite Element Modeling

7. *The FE models tended to overestimate transverse stiffness of the superstructure. Although there are numerous possible contributing causes for this, at least one possibility is that the relatively small spans between girders may admit significant shear deformation. Bridge researchers should consider the use of thin shell elements that incorporate shear deformations be used to model the slab.*
8. *A second possible source of overly stiff transverse behavior may be the degree of fixity assumed at the diaphragm to girder connections. Bridge researchers should explore the possible use of flexible connection models for these joints.*

9. *The FE models need to portray the bearing properties more accurately. Bridge researchers should undertake studies to develop efficient, yet accurate methods for modeling such properties.* These models need to be sufficiently versatile to permit modification as a part of structural model updating.
10. *Bridge researchers should conduct additional modeling studies directed toward accurately portraying pier stiffness.* Modeling considerations should include pier cap and column cracking, and possible footing rotation. A possible avenue to investigate might be to use plate elements to model the foundation and top flange of the pier rather than a series of beam elements. The plate elements might allow a better model of mass and stiffness distribution of the pier cap and still retain many fewer elements than the three-dimensional pier model.
11. *Bridge researchers need to explore more fully explicitly modeling the contributions of ancillary elements such as metal guardrails and bridge railings.*

## **BENEFITS AND IMPLEMENTATION PROSPECTS**

Implications of this study could have a significant effect on future health monitoring applications as they pertain to both curved and straight girder bridges. It is essential that finite element models in such long-term applications be able to reproduce the “as-built” response characteristics of a bridge. The current study raised significant issues about the ability to model the behavior of curved girder bridges correctly. Thus, it will be important to perform subsequent numerical research studies to develop models that will result in more precise predictions and to use these and other methods being developed in any health monitoring applications.

## **ACKNOWLEDGMENTS**

The work reported in this study was supported by a research grant from the Virginia Transportation Research Council. That support is gratefully acknowledged.

## **REFERENCES**

- Armstrong, W.M. (1972). Dynamic Testing of Curved Bridge-Huyck Stream. *Journal of the Structural Division*. ASCE. Vol. 98, No. ST9, pp. 2015-2030.
- Bendat, J.S. and Piersol, A.G. (1986). *Random Data: Analysis and Measurement Procedures*. John Wiley & Sons, Inc.; Second Edition (Revised and Expanded).
- Brigham, E.O. (1988). *Fast Fourier Transform and its Applications, The*. Prentice-Hall, Inc.

- Clark, C.B. (1966). Testing of a Model Curved Steel Girder Bridge. *Engineering Journal*. American Institute of Steel Construction. Vol. 13, No. 3, pp. 106-112.
- Christiano, P.P. and Culver, C.G. (1969). Horizontally Curved Bridges Subject to Moving Load. *Journal of the Structural Division*. ASCE. Vol. 95, ST8. 1615-1643.
- Colville, J. (1973). Tests of Curved Steel-Concrete Composite Beams. *Journal of the Structural Division*. ASCE. Vol. 99, ST7, pp. 1555-1570.
- Culver, C.G. and Christiano, P.P. (1969). Static Model Tests of Curved Girder Bridge. *Journal of the Structural Division*. ASCE. Vol. 95, ST8. 1599-1614.
- Dabrowski, R. (1968) *Curved Thin Walled Girders: Theory and Analysis*, Cement and Concrete Association, London.
- Ettouney, M., Hapij, A., and Gajer, R. (2001). Frequency-Domain Analysis of Long-Span Bridges Subjected to Nonuniform Seismic Motions. *Journal of Bridge Engineering*. ASCE. Vol. 6, No. 6, pp. 577-586.
- Farrar, C.R., Duffey, T.A., Cornwell, P.J., and Doebing, S.W. (1999) Excitation Methods for Bridge Structures, *Proceedings of the 17th International Modal Analysis Conference*, Kissimmee, FL.
- Hall, D.H. (1996). Curved Girders are Special. *Engineering Structures*. Elsevier Science Ltd. Vol. 18, No.10, pp. 769-777.
- Humar, J.L. (1990). *Dynamics of Structures*. Prentice-Hall, Inc.
- Linzell, D., Hall, D., and White, D., (2004). Historical Perspective on Horizontally Curved I Girder Bridge Design in the United States, *Journal of Bridge Engineering*. ASCE. Vol. 9, No. 3, pp. 218-229.
- Littler, J.D. (1995). An Assessment of Some of the Different Methods for Estimating Damping from Full-Scale Testing. *Journal of Wind Engineering and Industrial Aerodynamics*, Vol. 57. Elsevier Science Ltd., pp. 179-189.
- Lydzinski, J. (2006). *Finite element Analysis of a Multispan Horizontally Curved Girder Bridge*. University of Virginia. Charlottesville, VA.
- Maia, N.M.M., and e Silva, J.M.M., (editors), (1997) *Theoretical and Experimental Modal Analysis*, Research Studies Press Ltd., Baldock, England.
- McConnell, K.G. (1995). *Vibration Testing: Theory and Practice*. John Wiley & Sons, Inc.

- McElwain, B.A. and Laman, J.A. (2000). Experimental Verification of Horizontally Curved I-Girder Bridge Behavior. *Journal of Bridge Engineering*. ASCE. Vol. 5, No. 4, pp. 284-291.
- Palm, W.J. III (2001). *Introduction to MatLab 6 for Engineers*. McGraw-Hill. New York, NY.
- Ren, W-X., Zhao, T. and Harik, I.E. (2004). Experimental and Analytical Modal Analysis of Steel Arch Bridge. *Journal of Structural Engineering*. ASCE. Vol. 130, No. 7, pp. 1022-1031.
- Roll, F., and Aneja, I. (1966). Model Tests of Box-beam Highway Bridges with Cantilevered Deck Slabs, ASCE Transportation Engineering Conference, Philadelphia, PA, October 17-21.
- Senthilvasan, J., Thambiratnam, D.P., and Brameld, G.H. (2002). Dynamic Response of a Curved Bridge Under Moving Truck Load. *Engineering Structures*. Elsevier Science Ltd. Vol. 24, pp. 1283-1293.
- Shanmugam, N.E., Thevendran, J.Y., Liew, R., and Tan, L.O. (1995). Experimental Study on Steel Beams Curved in Plan. *Journal of Structural Engineering*. ASCE. Vol. 121, No. 2, pp. 249-259.
- Soto, M.H. (1966). Analysis of a Suspended Curved Girder. *Journal of the Structural Division*. ASCE. Vol. 92, No. ST1, pp. 21-38.
- Turnage, R.S. (2007) *Vibration testing of the Wolf Creek curved girder bridge*. M.S. Thesis, University of Virginia, Charlottesville.
- Virginia Department of Transportation (2001). *Road & Bridge Standards*, Volume III. Richmond.
- Womack, K. Halling, M. and Bott, S. (2001) *Static and Dynamic Testing of a Curved Steel Girder Bridge in Salt Lake City, Utah*, Report No. UT-00.13, Utah Department of Transportation Research Division, August.
- Yen, W-H. Phillip (1992). *Modal Identification of Bridge Structures*. University of Virginia. Charlottesville, VA.
- Zivanovic, S., Pavic, A., and Reynolds, P. (2005). Modal Testing and FE Model Tuning of a Lively Footbridge Structure. *Engineering Structures*. Elsevier Science Ltd., Vol. 28, pp. 857-868.
- Zureick, A., Lindzell, D., Leon, R.T., and Burrell, J. (2000). Curved Steel I-Girder Bridges: Experimental and Analysis Studies. *Engineering Structures*. Elsevier Science Ltd., Vol. 22, pp. 180-190.

Zureick, A., and Naqib, R. (1999). Horizontally Curved Steel I-Girders State-of-the-Art Analysis Methods. *Journal of Bridge Engineering*, Vol. 4, No. 1, pp. 38-47.



APPENDIX: PINNED RAIL MODE SHAPES 1-20

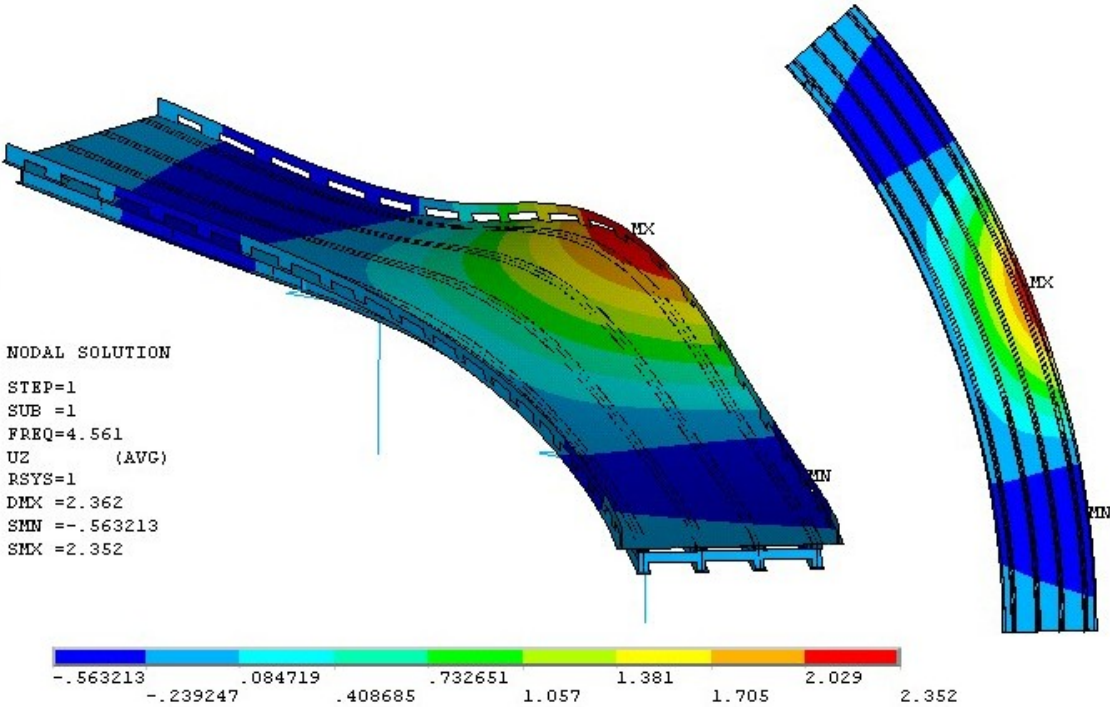


Figure A.1. Pinned Rail Model - First Mode – 4.561 Hz.

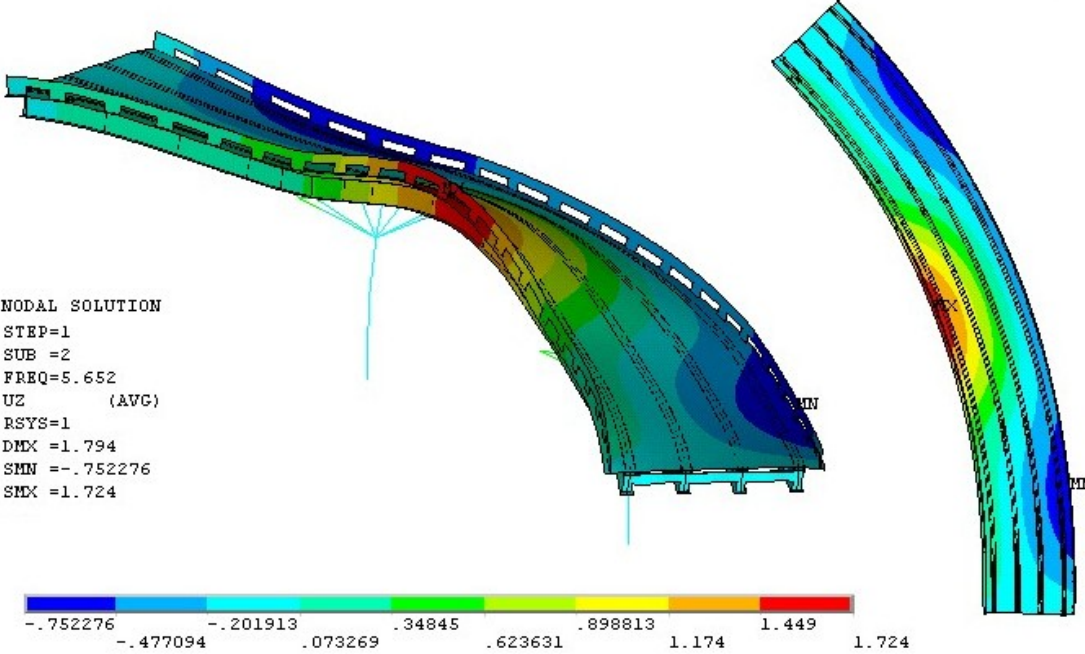


Figure A.2. Pinned Rail Model – Second Mode – 5.652 Hz

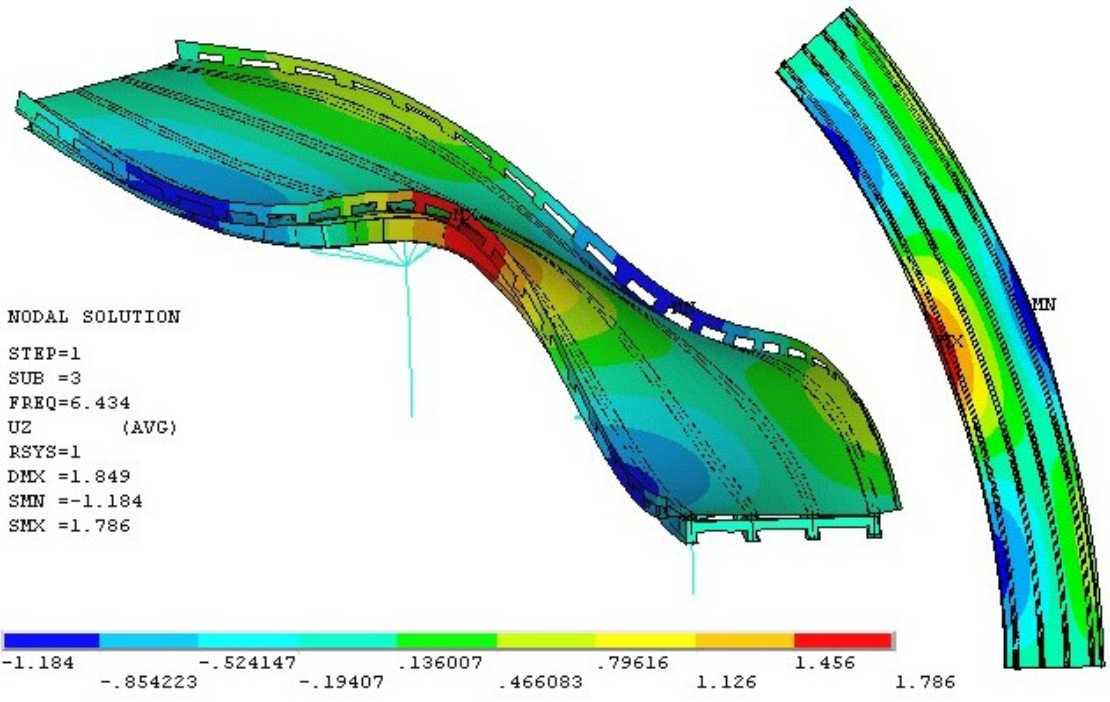


Figure A.3 Pinned Rail Model – Third Mode 6.434 Hz

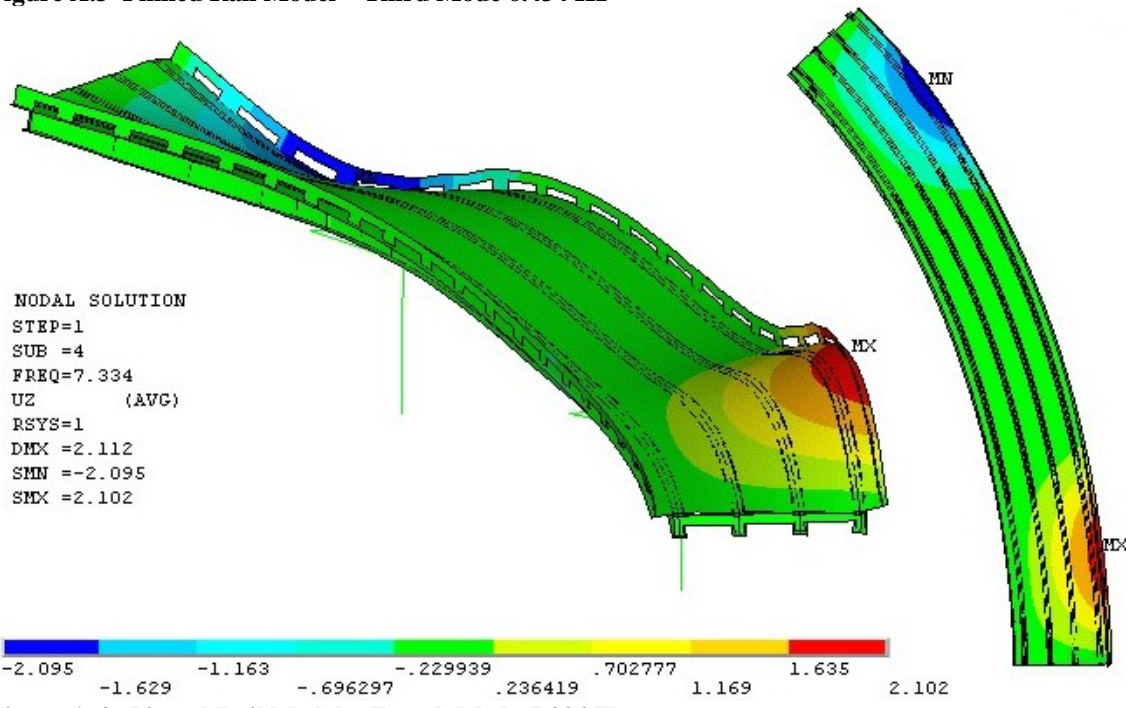


Figure A.4. Pinned Rail Model – Fourth Mode 7.334 Hz

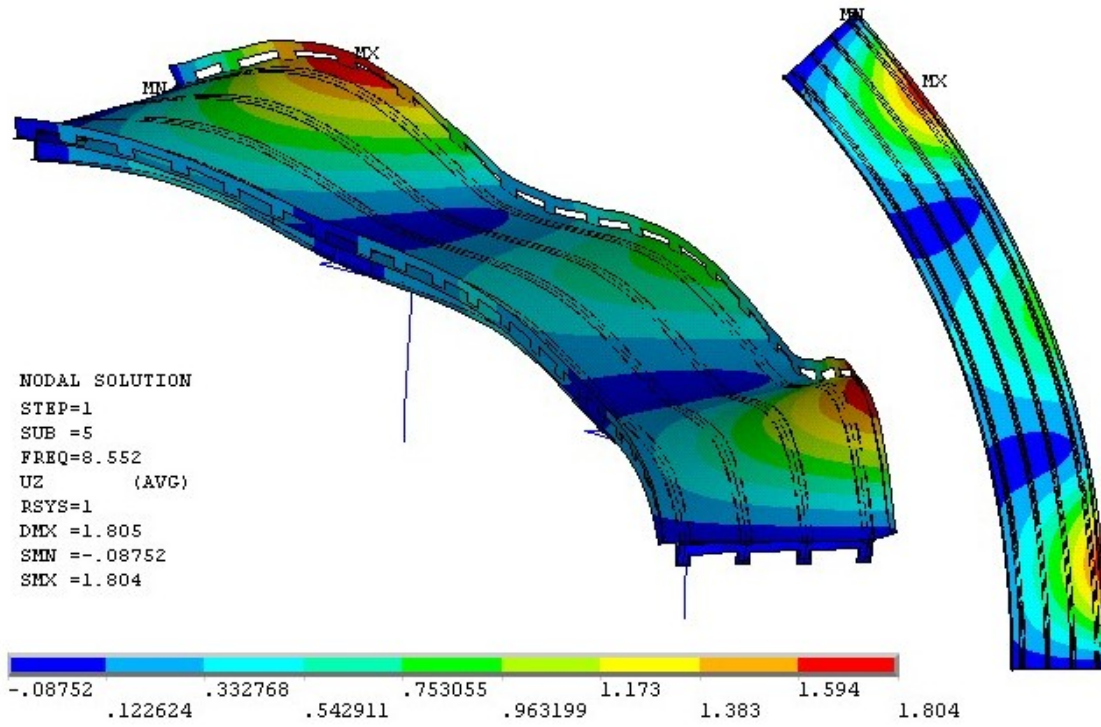


Figure A.5. Pinned Rail Model – Mode 5, 8.552 Hz

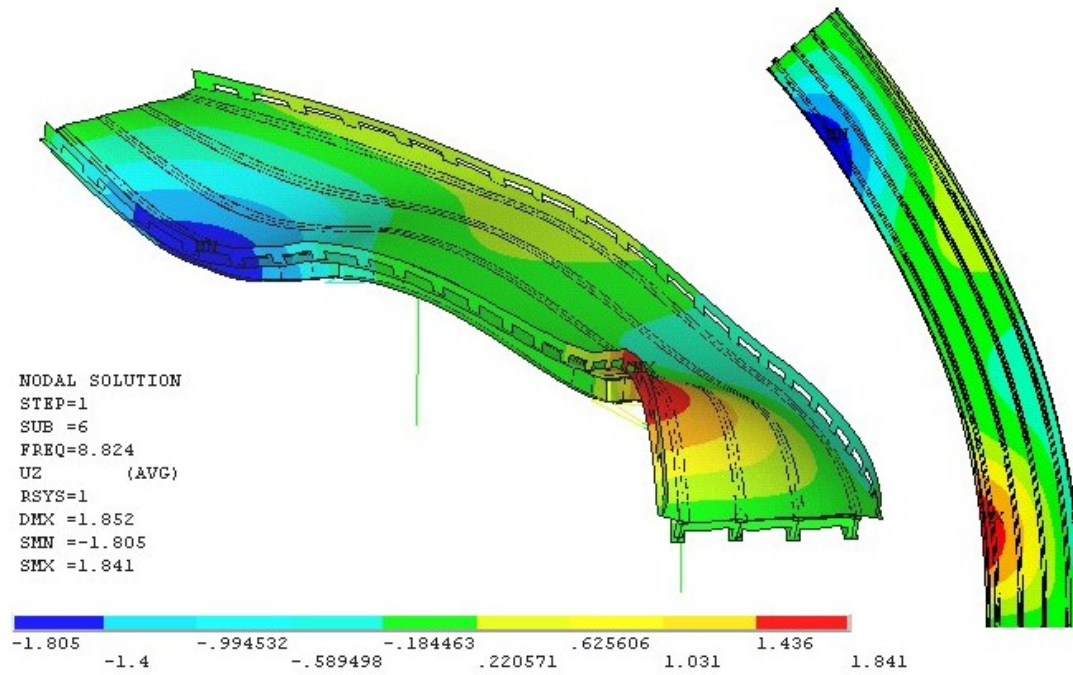


Figure A.6. Pinned Rail Model – Mode 6 - 8.824 Hz

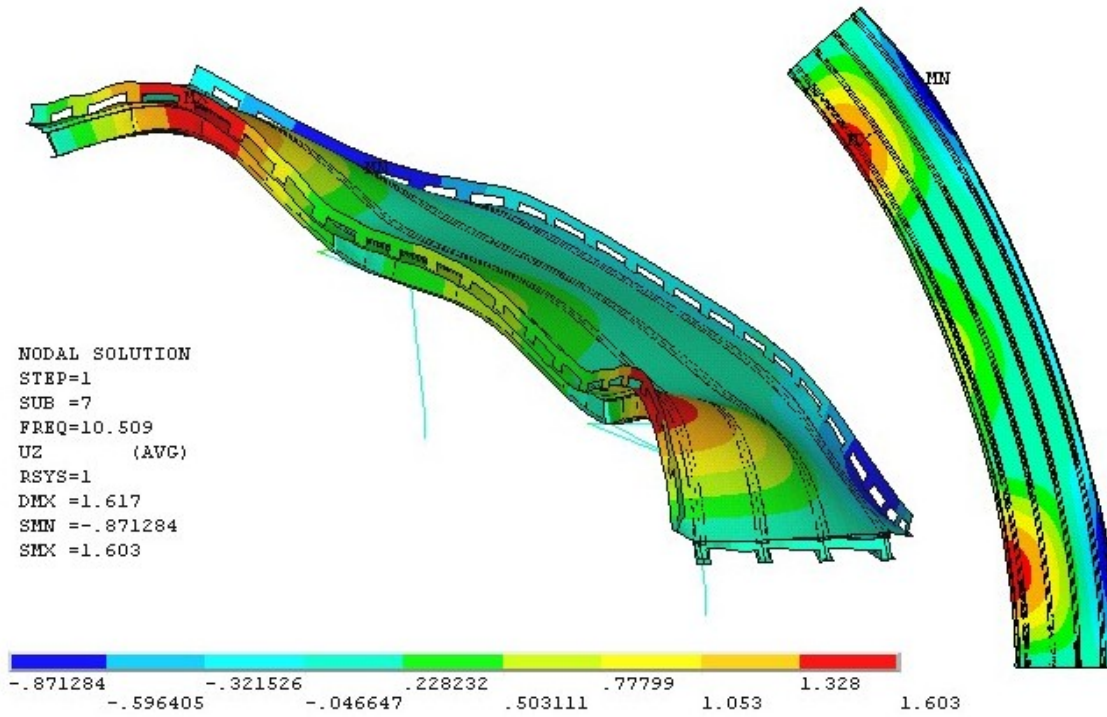


Figure A.7. Pinned Rail Model – Mode 7 – 10.509 Hz

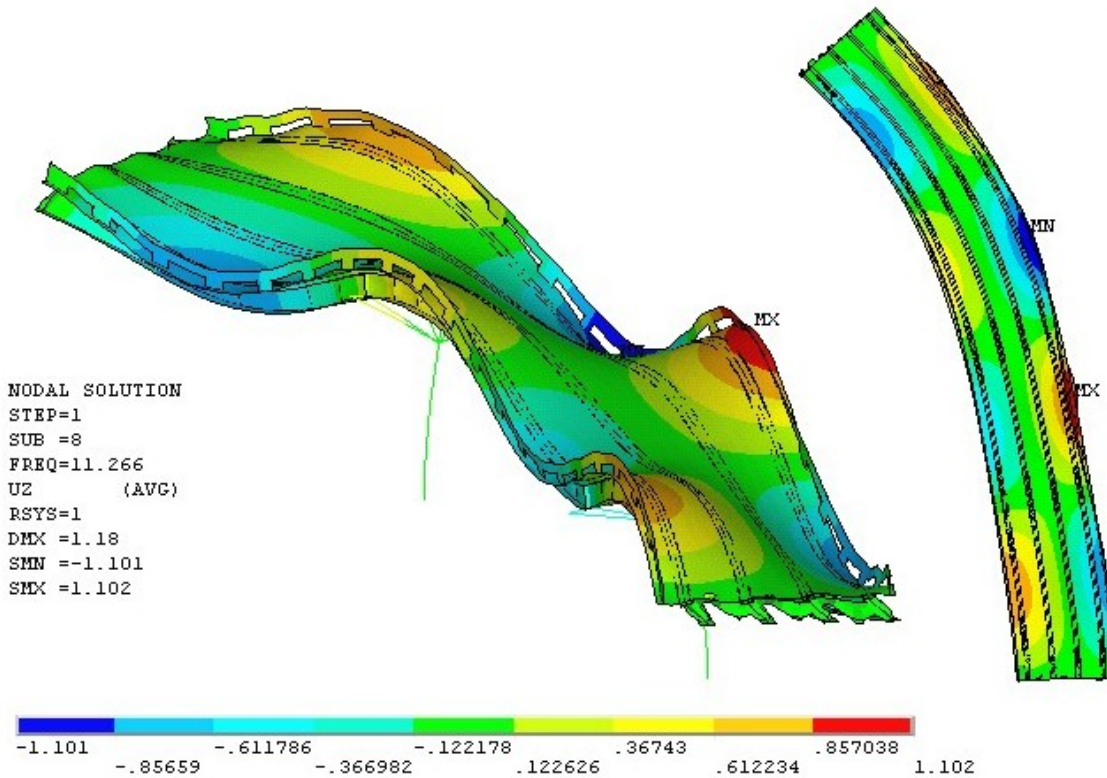


Figure A.8. Pinned Rail Model – Mode 8 – 11.266 Hz

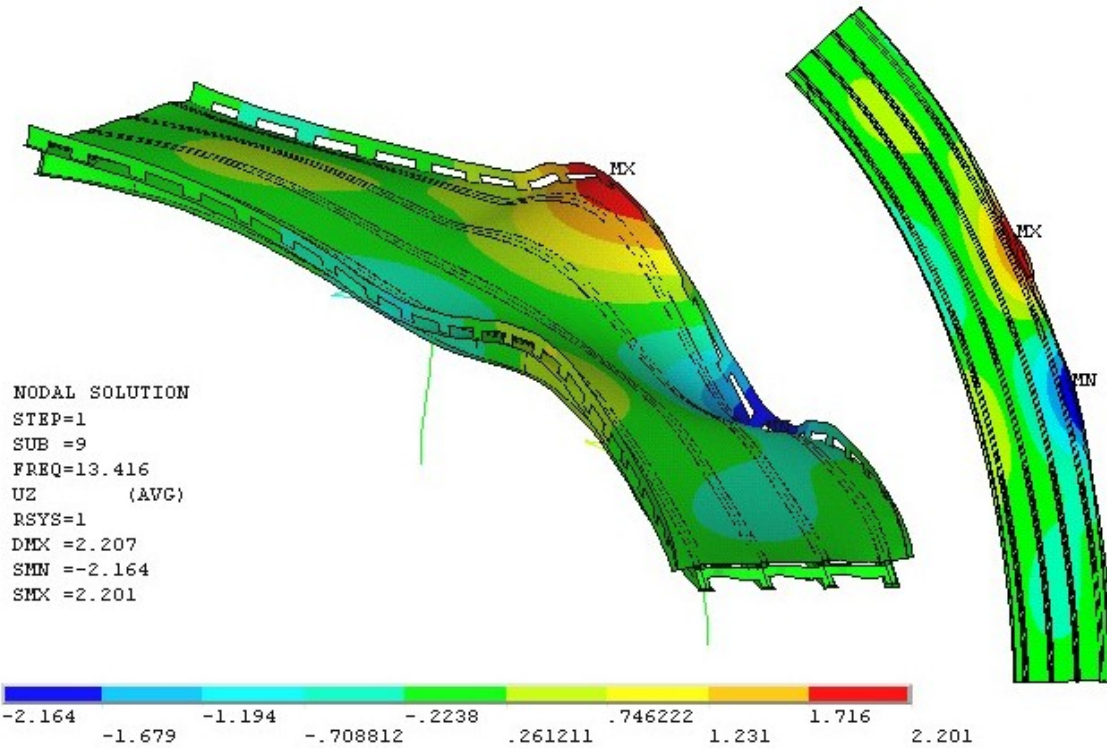


Figure A.9. Pinned Rail Model – Mode 9 – 13.416 Hz

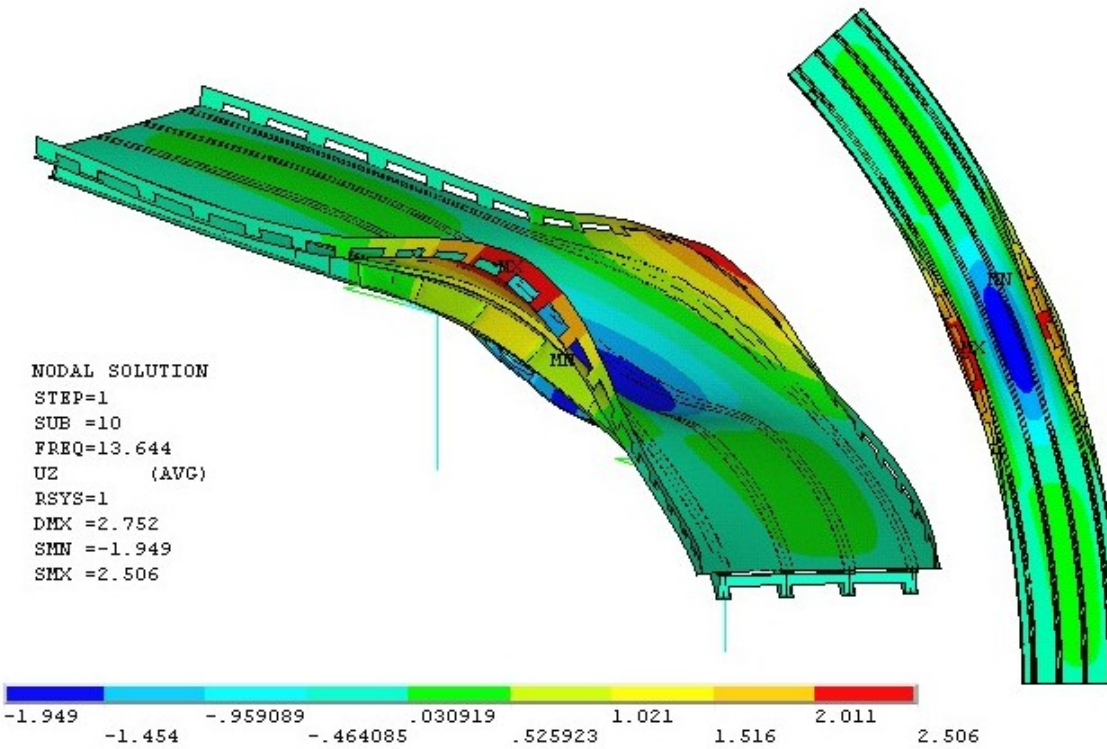


Figure A.10. Pinned Rail Model – Mode 10 – 13.644 Hz

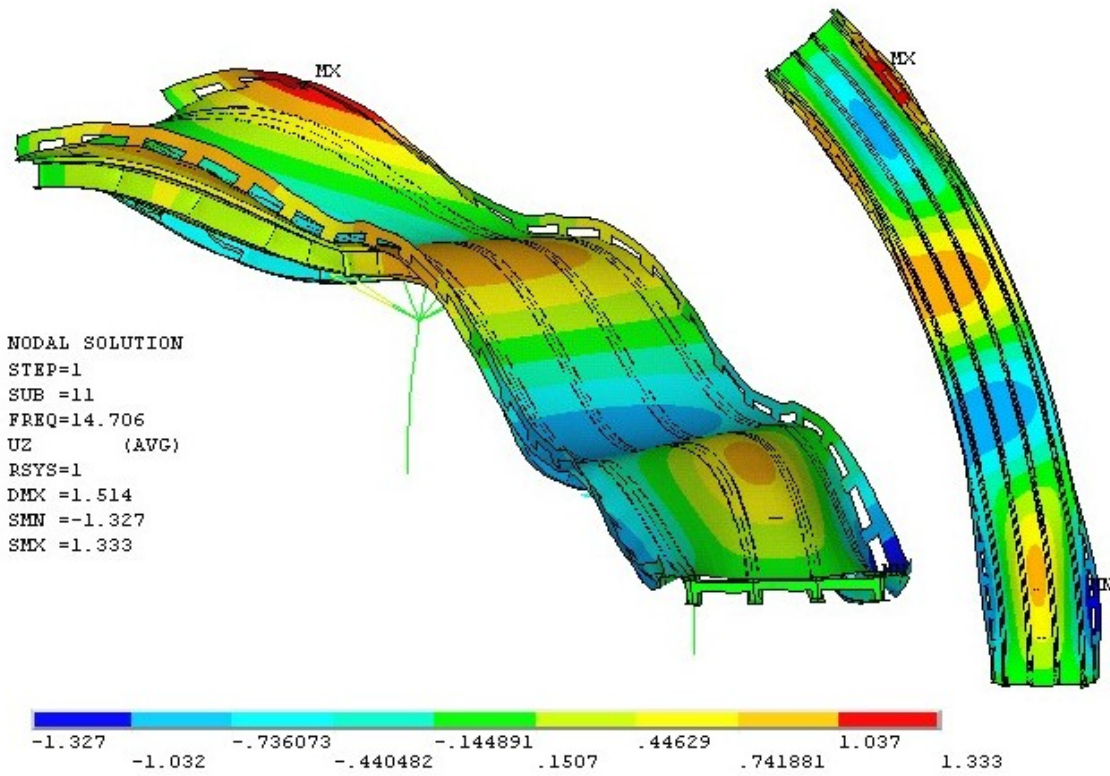


Figure A.11. Pinned Rail Model – Mode 11 – 14.706 Hz

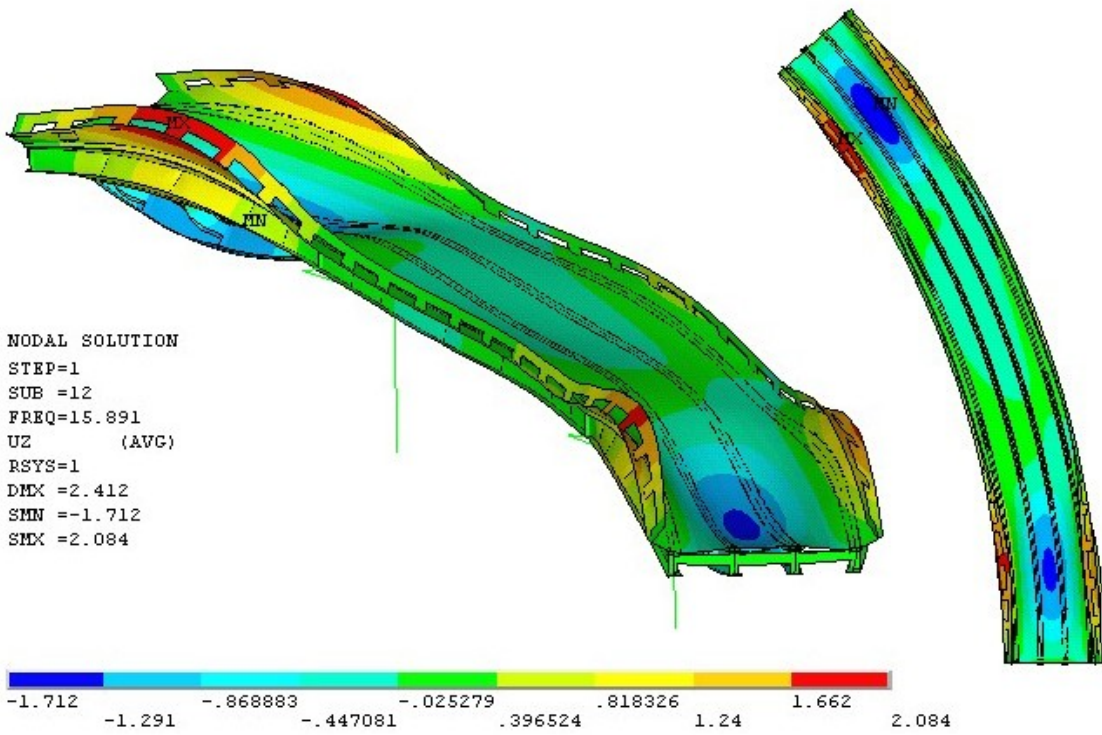


Figure A.12. Pinned Rail Model – Mode 12 – 15.891 Hz

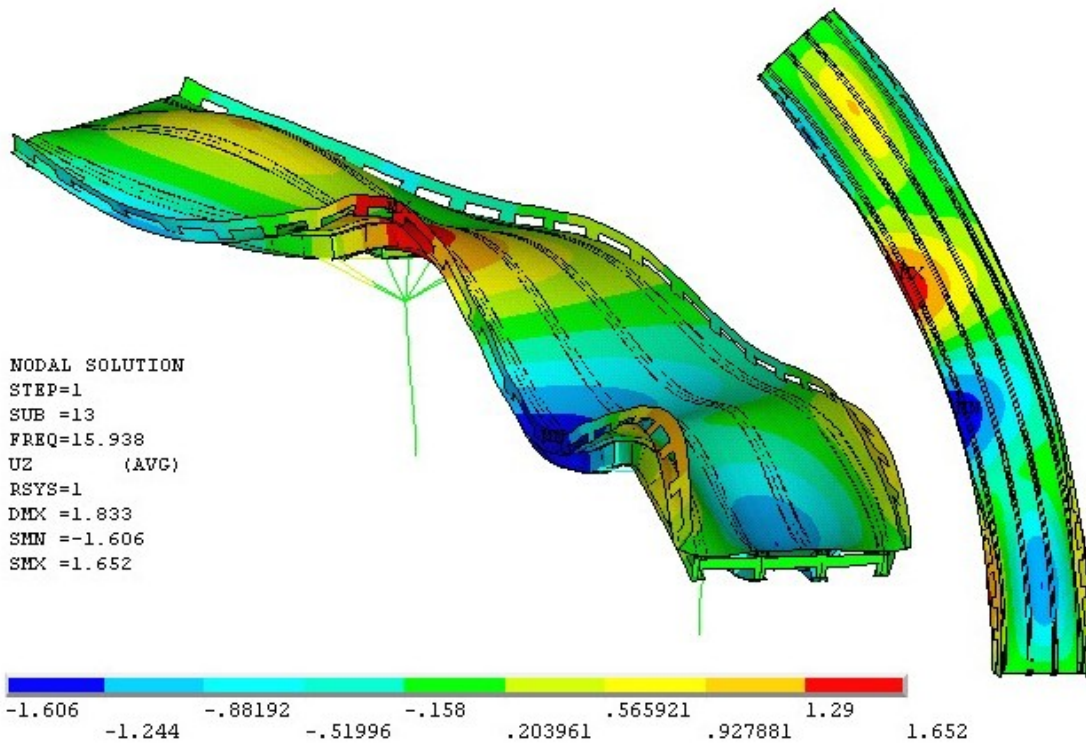


Figure A.13. Pinned Rail Model – Mode 13 – 15.938 Hz

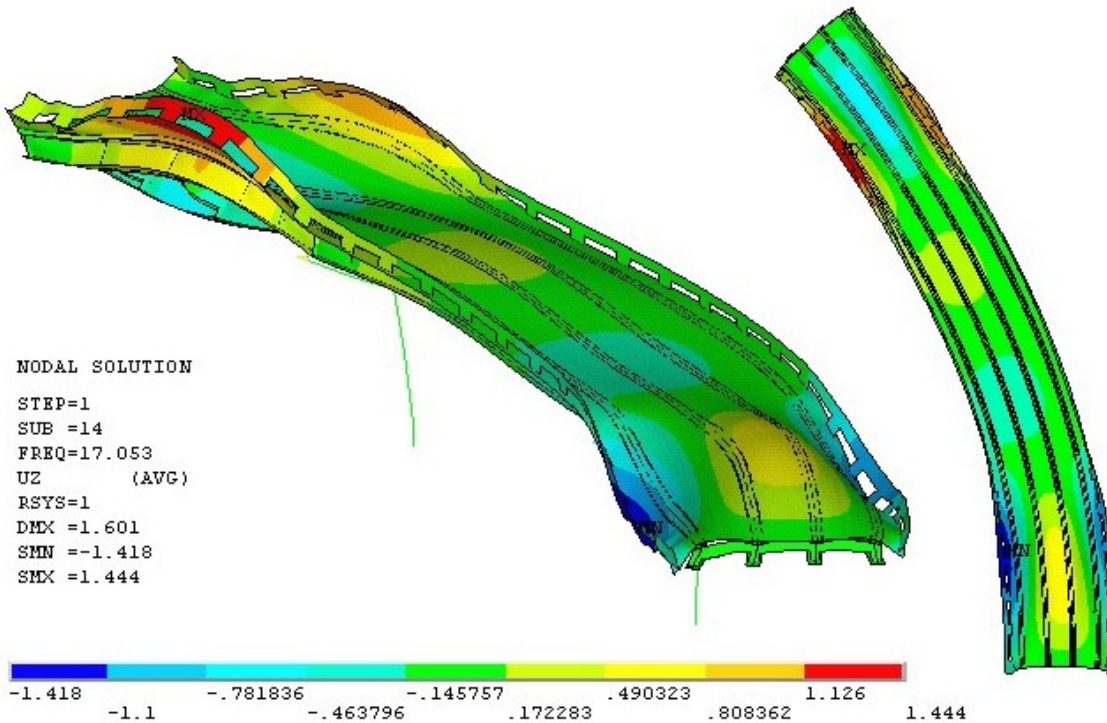


Figure A.14. Pinned Rail Model – Mode 14 – 17.053 Hz

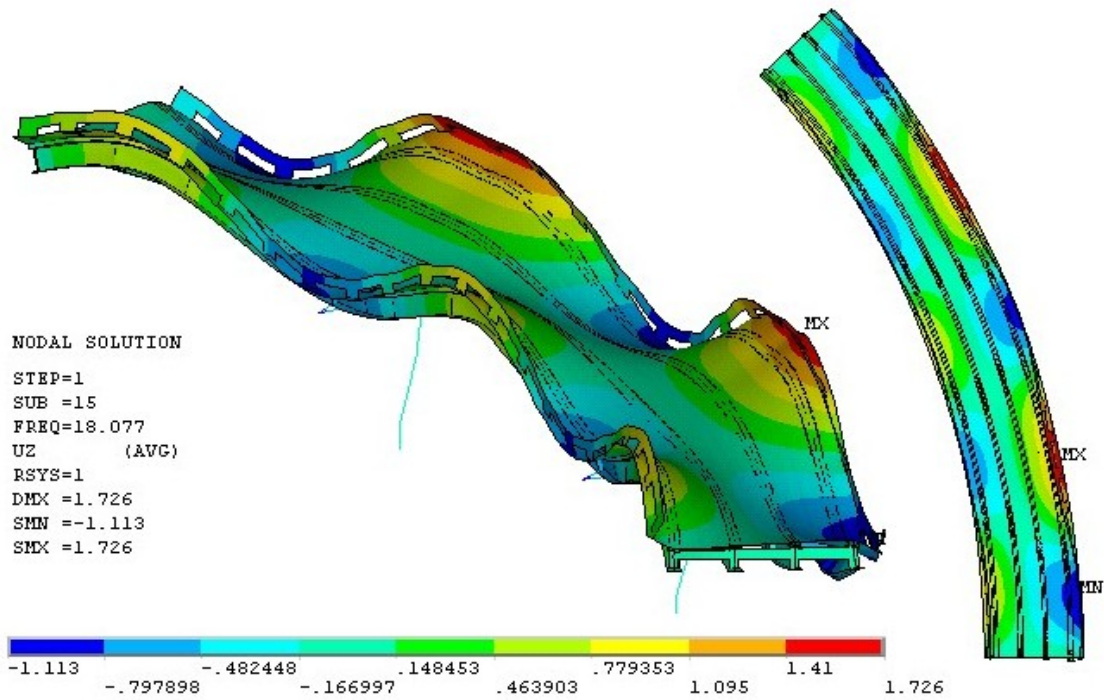


Figure A.15 Pinned Rail Model – Mode 15 – 18.077 Hz

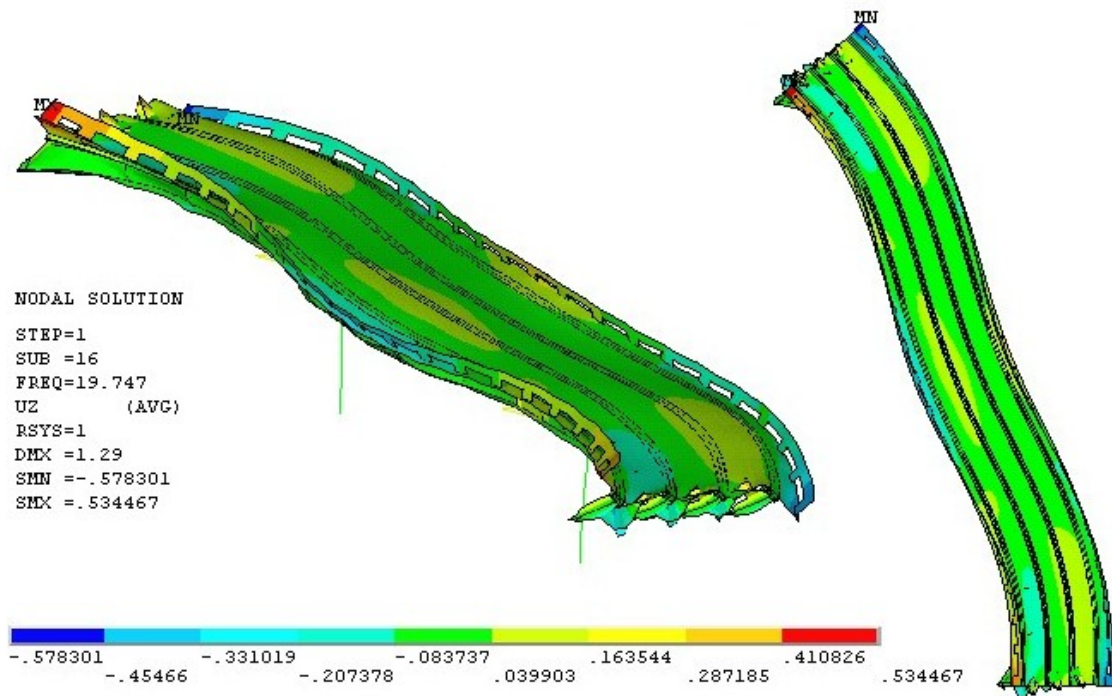


Figure A.16. Pinned Rail Model – Mode 16 19.747 Hz

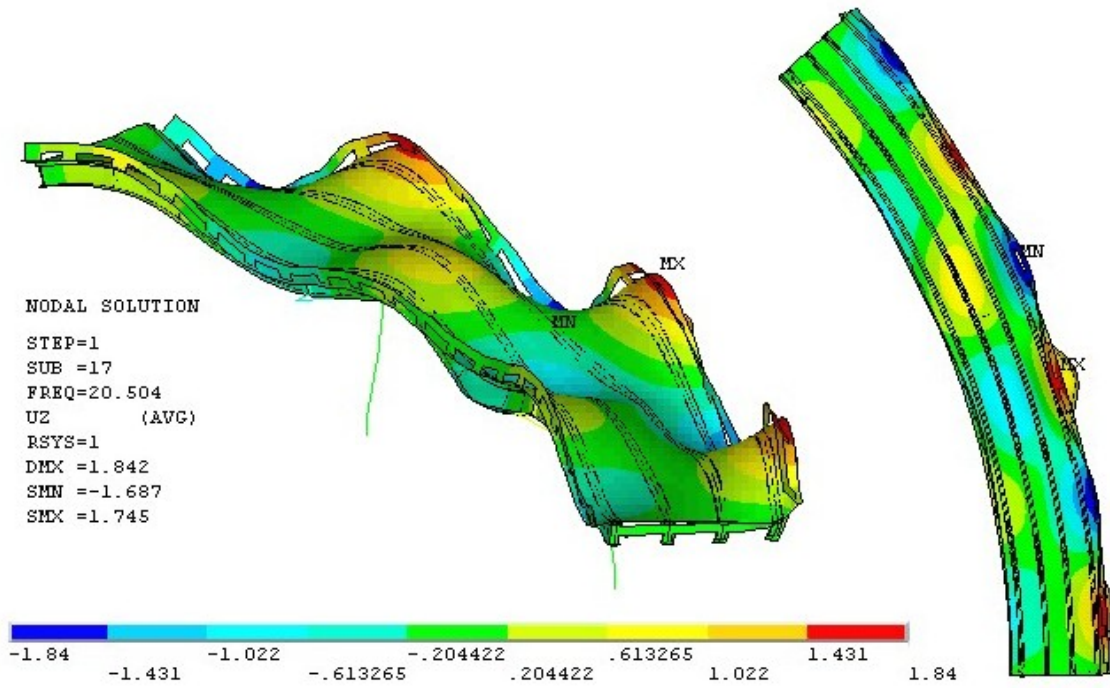


Figure A.17. Pinned Rail Model – Mode 17 – 20.504 Hz

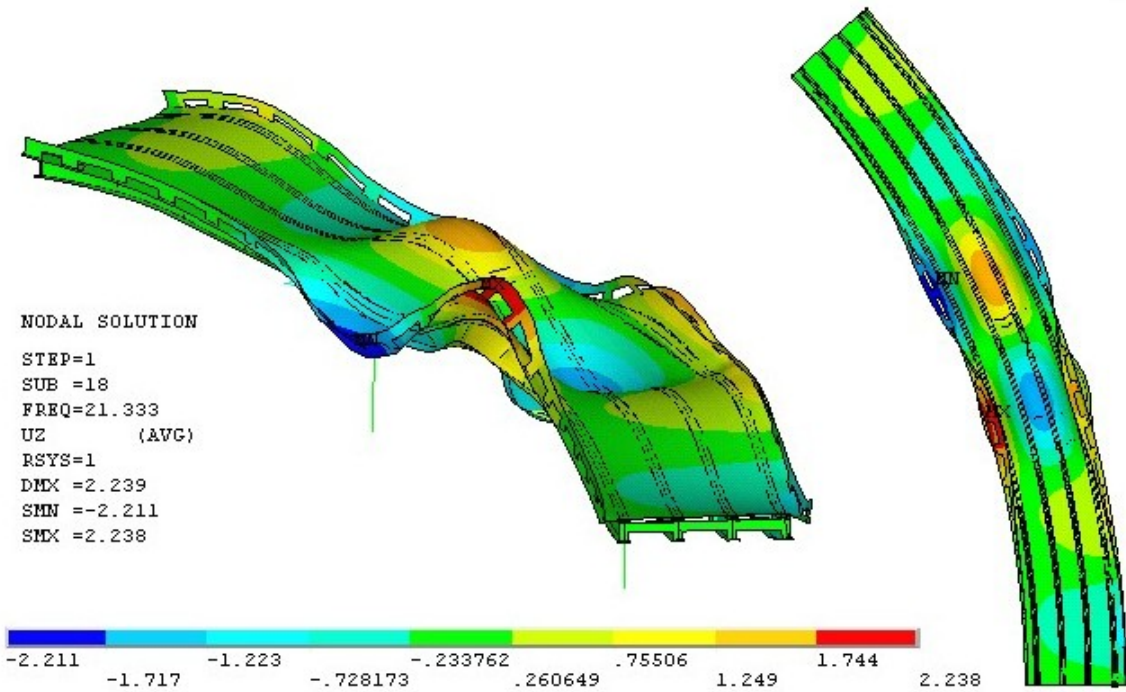


Figure A.18. Pinned Rail Model – Mode 18 – 21.333 Hz

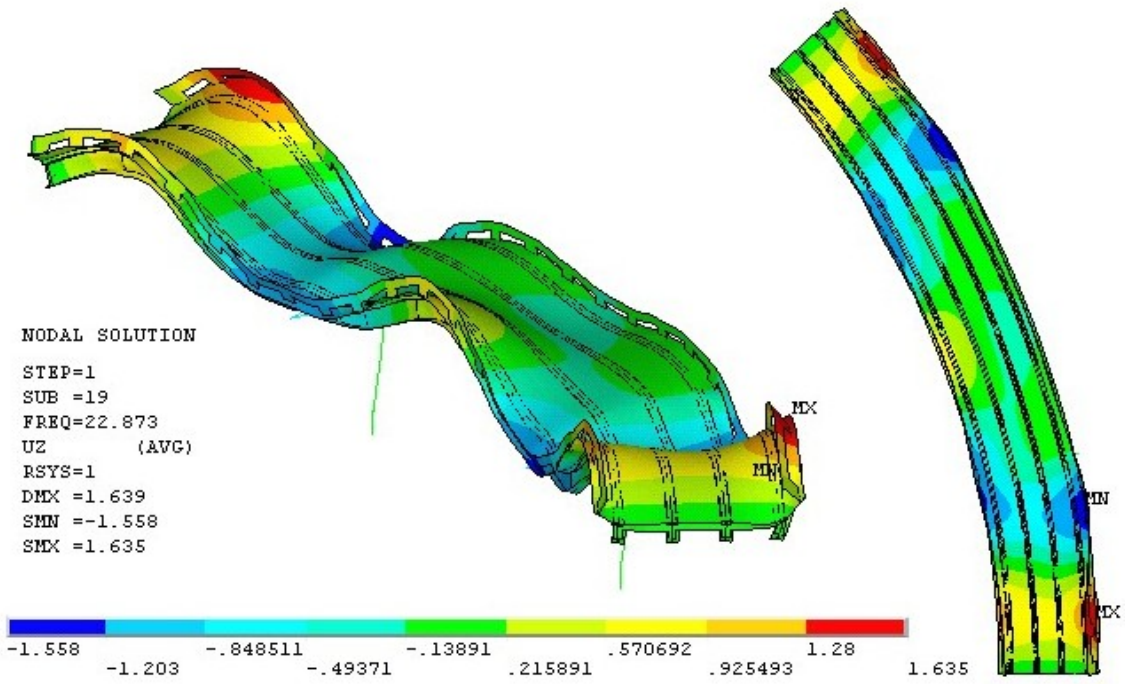


Figure A.19. Pinned Rail Model – Mode 19 – 22.873 Hz

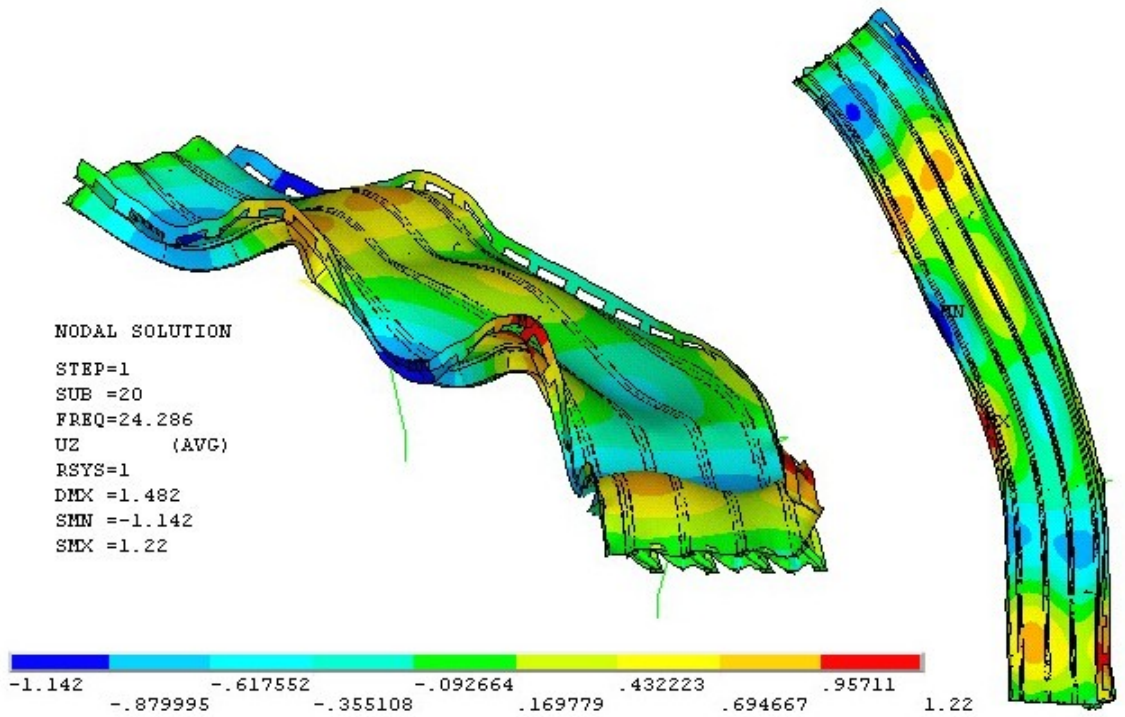


Figure A.20. Pinned Rail Model – Mode 20 – 24.286 Hz